CENTRO DE INVESTIGACIONES
EN OPTICA, A.C.

“REDUCTION OF GRAPHENE OXIDE AND ITS IMPACT ON THE PERFORMANCE OF A BIOSENSING SYSTEM”

Tesis para obtener el grado de Maestro en Ciencias (Óptica)

Presenta: Diana Lorena Mancera Zapata

Director de Tesis: Dr. Eden Morales Narváez

León · Guanajuato · México
Agosto de 2020

TABLE OF CONTENTS

LIST OF FIGURES

LIST OF TABLES

ACKNOWLEDGEMENTS

In the first place, I must thank my mother and brother. For always cultivating in me good habits and feelings, for seeking and wishing for the best for me; and, for always not only supporting but comforting me, even in the distance. Thank you for being my role models and my inspiration to move forward.

To my childhood friends, for being interested and have listened to my conversations about science without getting bored. The friends I have met along the way and driven me to move on. To those friends who, during the time of this master's degree became my family and who I will miss when the day they should leave arrives.

I would like to thank Gus for being my constant support, my ground pole and fighting partner, thank you for always being unconditional.

I could not continue without thanking my advisor, Dr. Eden Morales, for accepting me into his group, for his patience and trust. For constantly seeking to enhance my abilities and teaching me that love for science involves effort and dedication, that, as in life, in science things must always be done well.

To my group's colleagues for their warmth and willingness to solve my doubts.

Finally, even if he is not quite aware of the situation, I would like to thank Milo, my dog. The one who went through the countless and sleepless nights with me while I was in the process of making the thesis.

Finally, I would like to express my acknowledgement to CONACYT for financial support.

Thank you everyone!

ABSTRACT

Graphene oxide (GO) has aroused the interest of the scientific community due to its extraordinary properties and potential applications; for example, in biosensors, which are analytical devices that can detect the presence of target molecules with high specificity and sensitivity.

Particularly, GO has been demonstrated to be an excellent photoluminescence quencher, this property is very useful in the development of biosensing systems based on fluorescence resonance energy transfer (FRET). Additionally, it has been reported that the effect of fluorescence quenching is more efficient when GO is reduced. This effect could be directly used to enhance the analytical performance of a FRET–based biosensing system.

In the present thesis, the effects generated in the analytical performance of a biosensing platform due to the reduction of GO in three different samples are reported. This study was divided into several stages, the first one consisted of making GO adhesion tests on the surface of tissue culture treated (TCT) microplates, this in order to know the approximate amount of GO that adheres to the surface after stages of washing with ultrapure water, the results of this stage reveals that around 5 % of the concentration of GO used to cover the TCT microplates surface remains on it after the washing stages. This information is relevant to the next stage, because the amount of reducing agent, L-ascorbic acid (L-AA) will depend on this, since the suggested amounts of L-AA correspond to 1.75 and 3.5 times the concentration of GO (1.75x [GO] and 3.5x [GO]). Once the reduction process was performed on GO, photoluminescence quenching studies were performed, and these studies indicated that, effectively, the reduction process generated changes in quenching values (ratio between final and initial intensity, I_0/I_f) from 0.32 to 0.40, and the photoluminescence quenching saturation time from 32 to 25.68 minutes for GO and rGO respectively. Additionally, the samples 4.1 GO and 4.1 rGO, displayed better adhesion and so enhance their abilities as a

fluorescence quencher when high binding surface microplate surface was employed. The changes of fluorescence quenching values were 0.74 and 0.40, 0.71 and 0.38 for 4.1GO and 4.1rGO samples, respectively. In 5.1 case the fluorescence quenching values were 0.68 and 0.39, 0.69 and 0.37 for 5.1 GO and rGO respectively.

Nowadays, biosensors have become indispensable tools for many fields, so it is necessary to have reliable and efficient devices.

This work is highly relevant since the results presented here represent a first advance to establish parameters that contribute to improving the analytical performance of a biosensing platform, generating increasingly efficient devices in terms of sensitivity and assay time.

General Objective

The main objective of this thesis is to evaluate the impact of the reduction of graphene oxide on the analytical performance of a FRET-based biosensing platform.

Specifics Objectives

- To perform studies of GO adhesion to determine the quantity of GO adhered onto microwell plates.
- To carry out reduction process in GO-decorated microwell plates.
- To employ Raman spectroscopy to characterize the reduction process of GO.
- To optimize a FRET-based biosensing platform using reduced GO.
- To evaluate the analytical performance of a FRET-based biosensing platform targeting human Immunoglobulin-G (IgG).

Collaborative Publications in the Framework of This Thesis

- **Front cover of Analytical Chemistry (upcoming issue, September 1, 2020).** *Image concept by Diana L. Mancera-Zapata, Mariana D. Avila-Huerta and Eden Morales-Narváez. Image created by Diana L. Mancera-Zapata.*

- **Real-Time Photoluminescent Biosensing Based on Graphene Oxide-Coated Microplates: A Rapid Pathogen Detection Platform.**
  Mariana Avila-Huerta, Edwin J. Ortiz-Riaño, Diana L. Mancera-Zapata, E. Morales-Narváez. Analytical Chemistry (2020), DOI: 10.1021/acs.analchem.0c02200

- **Microwell plates coated with graphene oxide enable advantageous real-time immunosensing platform.**
  Edwin J. Ortiz-Riaño, Mariana Avila-Huerta, Diana L. Mancera-Zapata, E. Morales-Narváez. Biosensors and Bioelectronics, 112319 (2020), DOI: 10.1016/j.bios.2020.112319

Important Note

The experimental development of this thesis was affected by the health contingency situation the world is going through due to COVID-19. Some of the experiments scheduled for 2020 could not be carried out.

The objectives (mentioned above) that could be achieved totally or partially will be detailed below.

The study of GO adhesion onto microplate surface, the GO reduction process and its characterization using Raman spectroscopy could be performed, as well as an optimization of other reagents (such as the IgG-FITC photoluminescence probes).

However, part of our interest was to determine under which concentrations and reduction levels the changes in the sensitivity and response time of the biosensing platform became optimal. This exploration process was not possible because the access of laboratory has been totally restricted, since March 17 of 2020 and continues until current date (early August 2020).

In conclusion, the specific objectives were carried out, however to generate a more consistent study on the effects of the rGO on the analytical performance of the biosensing system, it is required to perform these same experiments but considering other conditions and parameters.

INTRODUCTION

Due to its advantageous properties, graphene oxide (GO) has been widely used in the biosensing field. One of the most promising property of GO for this field is the photoluminescence quenching ability. [1]

Using GO as a fluorescence quencher and bearing in mind the hypothesis that reduced graphene oxide favors the analytical performance of a FRET-based biosensing system by means of a more efficient quenching of fluorescence, we developed a biosensing platform using GO and rGO as acceptors to optimize the sensitivity/assay time of a FRET-based biosensing. L- ascorbic acid (L-AA) is used for the reduction process since L-AA has a mild reductive ability and nontoxic property.

This thesis is divided in five fundamental chapters designed to describe all the important aspects involved in the study of the analytical performance of a GO/rGO-FRET-based biosensing platform.

Chapter 1. Theoretical framework: This chapter is devoted to offer an overview on key concepts such as a biosensor, photoluminescence, FRET, G and GO and rGO. Particular features on these concepts will be discussed in this section.

Chapter 2. State-of-the-art of FRET-GO/rGO based biosensors: This chapter is dedicated to analyze the state-of-the-art regarding GO-FRET-based biosensors. It is important to be aware of the research that is currently being done around this topic in order

to know what kind of contribution is possible to generate by means of this thesis.

Chapter 3. Experimental set up: Herein, it is offered a description of the experimental procedures that were performed to study the impact of GO reduction on the sensitivity/assay time of a biosensing system.

Chapter 4. Discussion and results: This chapter presents the analysis of the results of the experiments carried out in the previous chapter. The analysis of results is important since it allows defining which parameters are relevant to achieve the objective of the work.

Chapter 5. Conclusions: Overall Conclusions resulting from this thesis as well as the corresponding contributions are summarized.

CHAPTER 1.

THEORETICAL FRAMEWORK

1.1.Definition of a biosensor

Biosensors are analytical devices that can detect the presence of target molecules with high selectivity and sensitivity. The selectivity in a biosensor is directly related to the ability of an analytical procedure to detect a specific analyte between several substances in a sample, this feature is of great importance since biosensors with low selectivity tend to generate false positives, causing limited reliability and low efficiency in biomedical applications, since biological samples are composed of numerous types of analytes that can be confused as the target bioanalyte. [2] It is important to clarify that the concept of selectivity is frequently used interchangeably with the concept of specificity, however, UIPA (International Union of Police Associations) indicates: "A specific reaction or test is one that occurs only with the substance of interest, while a selective reaction or test is one that can occur with other substances but exhibits a degree of preference for the substance of interest. Few reactions are specific, but many exhibit selectivity". [3]

On the other hand, biosensor sensitivity is related to the generation of a transduced signal due to changes in the concentration of the bioanalytes. Biosensors with high sensitivity have the ability to generate a signal from small fluctuations in the concentration of the

bioanalytes. The minimum and maximum amount of analyte that can be detected by a biosensor defines its limit of detection (LOD) or sensitivity. In a biosensing system, sensitivity can play an important role, for example, in biomedicine a device with high sensitivity can obtain early diagnosis of diseases. [3]

The basic principle of biosensors involves three stages (*see Figure 1*), the first one consists in the biological recognition or biorecognition which must be highly specific. The next stage is the transduction process and it consists in the transformation of a biological activity in a quantifiable signal to obtain information about changes of a certain physical magnitude, for example, fluorescence intensity, pH changes, etc. Finally, the signal out is obtained and interpreted. [4,5]

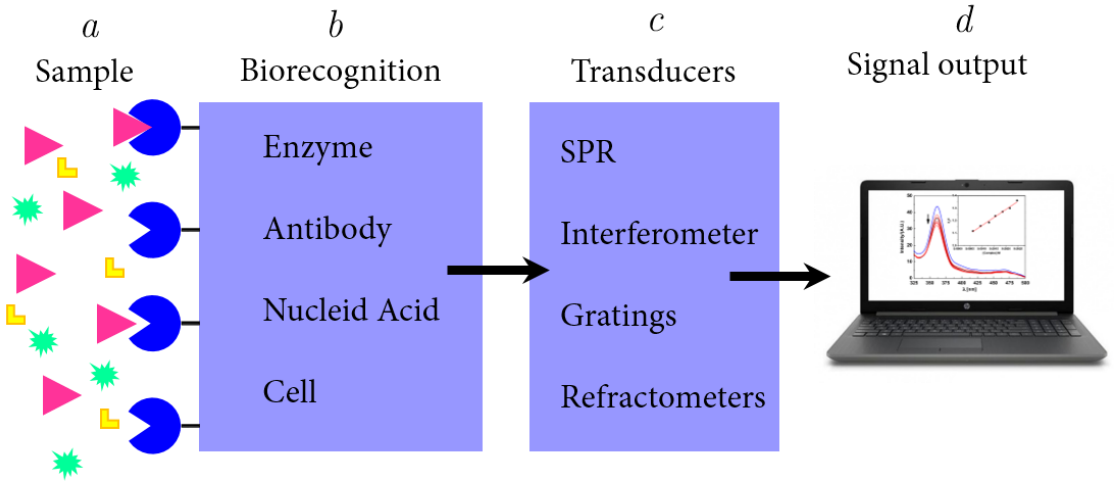

Figure 1 Principle of biosensor (Optical biosensor). a) Sample. Substance to be analyzed that is likely to contain the target analyte. b) Biorecognition. At this stage, molecular complexes (biorecognition elements) highly related to the analyte are required. c) Transduction unit. Device responsible for converting the measured biological activity in a signal quantified cable. d) Signal output. Measurable signal that contains the information of whether or not the analyte is present in the sample

1.2.Physical phenomena involved in FRET-based optical biosensing

1.2.1. Photoluminescence

Photoluminescence is the process in which the absorption of a photon by a molecule (fluorophore), excites its electrons, promoting them to excited state. The transition of this electron to its ground state is made through the emission of a photon.

Photoluminescence phenomenon is classified in two types, fluorescence and phosphorescence, which depends on the nature of the excited states. When a transition occurs between photoexcited specimens from their first excited singlet state to their ground state, we are talking about fluorescence, while phosphorescence is the emission of light from excited triplet states

When a substance passes to the excited state, it can go to the singlet state, an excited state in which all its electrons are paired and the total spin is zero, or to the triplet state, an excited state with a non-zero spin multiplicity.

The lifetime of fluorescence typically ranges in the order of nanoseconds while the lifetime of phosphorescence ranges in the order of milliseconds to seconds. This is because in fluorescence the absorbed energy is quickly released, the excited electrons return to the ground state almost instantly (ns). On the other hand, in phosphorescence phenomenon, typically, the energy is released slowly, the excited electrons go through the intersystem

crossing , passing through intermediate excited states that slow down the relaxation towards the ground state and thus the release of the absorbed energy, which allows the phosphorescent substances to continue emitting light, in some cases, for a few hours after photon absorption. [6]

The processes that occur between absorption and light emission are typically represented on a Jablonski diagram, (see figure 2).

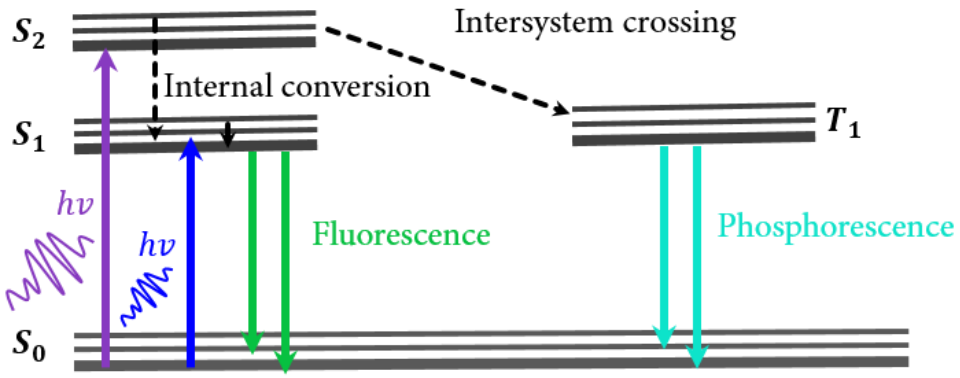

Figure 2 Typical Jablonski diagram to illustrate photoluminescent processes. The labels S_0, S_1 and S_2 refer to the baseline singlet state, first singlet excited states and second singlet excited states, respectively, similarly T_1 represents the first triplet excited state.

1.2.2. Fluorescence resonance energy transfer (FRET)

FRET is a widely used phenomenon in different fields such as medical diagnosis, biosensing systems, optical imaging, DNA analysis. It is also useful for measuring distances between molecules, protein interaction and many others applications. [7]

It is an electrodynamic phenomenon based on non-radiative transfer of energy between two molecules, an excited donor molecule and an acceptor molecule, the energy transfer can only occur if the emission spectrum of the donor overlaps the absorption spectrum of the

acceptor, that is, the vibrational transitions in the donor display the same energy as the corresponding transitions in the acceptor molecule (see Figure 3). [6]

In order to simplify FRET interpretation, it is interesting to contemplate the J. Perrin theory, where an excited molecule is considered as a classical mechanical oscillator and energy transfer as a mechanical coupling between two pendulums, where the pendulum set in motion (donor) transfers its energy to the second one (acceptor). [8]

It is important to note the abbreviation of FRET corresponds to fluorescence resonance energy transfer, this expression is a little confusing because it is not the fluorescence that is transferred but the resonance energy of the excited donor. [8] To avoid this situation, in certain literature, FRET is defined as Förster Resonance, energy transfer.

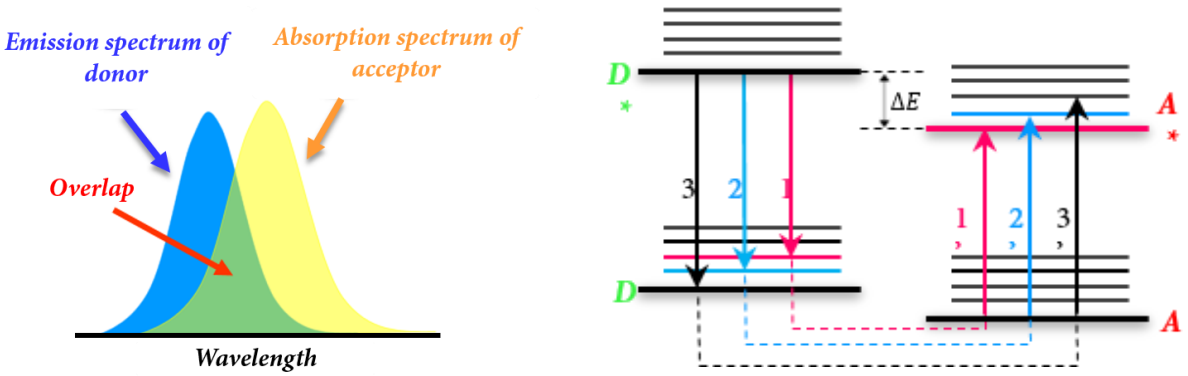

Figure 3 FRET a. Integral overlap between the emission spectrum of the donor and the absorption of the acceptor. b. Energy level scheme of donor and acceptor molecules showing the coupled transitions.

Energy transfer phenomenon can occur principally through two mechanisms, dipole-dipole interaction (Coulombic interaction) and intermolecular orbital overlapping (electron exchange)[7].

When resonance energy transfer (RET) occurs, the electron in the excited donor (D*) returns to the ground state. Simultaneously an electron in the acceptor (A) goes into a higher excited-state orbital. If the acceptor is fluorescent it may then emit. If the acceptor is no fluorescent the energy is dissipated by other mechanism, as heat for example. [9]

In general, the efficiency of RET depends to the sixth power of the distance between donor and acceptor and their relative orientation. [9] Typically, rate of transfer of excitation energy is given by the next expression:

$$\kappa_T(r) = \left(\frac{1}{\tau_d}\right)\left(\frac{R_0}{r}\right)^6 \qquad (1)$$

However, in the case of graphene, its nature as a 2 dimensional dipole modifies the expression (1) to an r^4 dependence. [10,11]

Here, τ_d is the fluorescence lifetime of the donor when the acceptor is absent, r is the distance between the centers of the donor of acceptor molecule and R_0 represents the distance at which 50% of the excitation energy is transferred to the acceptor, it is denoted as a Förster distance. [6] In RET, the distance is relatively large compared to the size of the molecule, so the energy transfer can be considered as a through-space interaction, that is, RET does not require molecular contact between donor and acceptor molecules. [12]

The resonance transition phenomenon is also related to the efficiency in energy transfer. Thus, the more overlap of spectra, a donor increases the possibility to transfer energy to the acceptor. [6] Overlap integral, J(λ), between the donor and the acceptor stands for the overlap

of spectra is given by

$$J(\lambda) = \int_0^\infty F_D(\lambda)\epsilon_A(\lambda)\lambda^4 d\lambda \qquad (2)$$

where $F_D(\lambda)$ is the normalized emission spectrum of the donor, $\epsilon_A(\lambda)$ corresponds to molar absorption coefficient of the acceptor and λ is the wavelength [6].

Non-radiative transfer has effects on the characteristics of fluorescence emission from the donor. If the distance between donor and acceptor is very small (few Angstroms), the molecules come into contact and the electron clouds of these molecules are able to interact.

The interactions between orbitals are usually called electron exchange because electrons can move between the molecules at short distances, [9] electron exchange is only one of several mechanisms for the fluorescence quenching, being fluorescence quenching defined by

$$I_f / I_0$$

This ratio represents the attenuation of fluorescence intensity in a specific time frame. Here I_f corresponds to the final intensity and I_0 corresponds to initial intensity.

1.2.3. Graphene, graphene oxide (GO) and reduce graphene oxide (rGO)

Graphene is a carbon material. Due to its atomic thickness, it is considered a 2D material. It can be described as a planar sheet with several carbon atoms organized in a honeycomb arrangement which is the primary structure to build the others carbon allotropes (see Figure

6). If at least 10 of graphene sheets are stacked, we can obtain a 3D structure known as graphite, 0D fullerenes if we wrap up a sheet or 1D nanotubes if we rolled it into. [13]

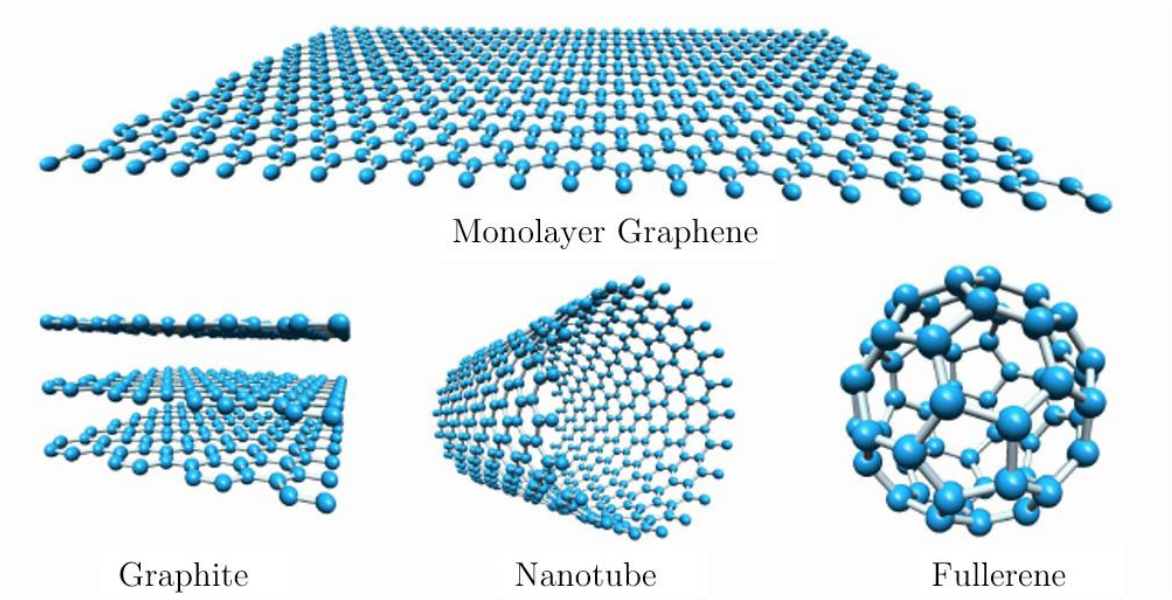

Figure 4 Some of Carbon allotropes. Adapted with permission. [14] Copyright © 2012, Springer Nature.

In order to understand more about the graphene structure, it is important to know the electronic configuration of the carbon atom and the different types of bonding involved. Figure 5 shows the electronic configuration of carbon in the ground states, excited state and sp^2 hybridization.

.

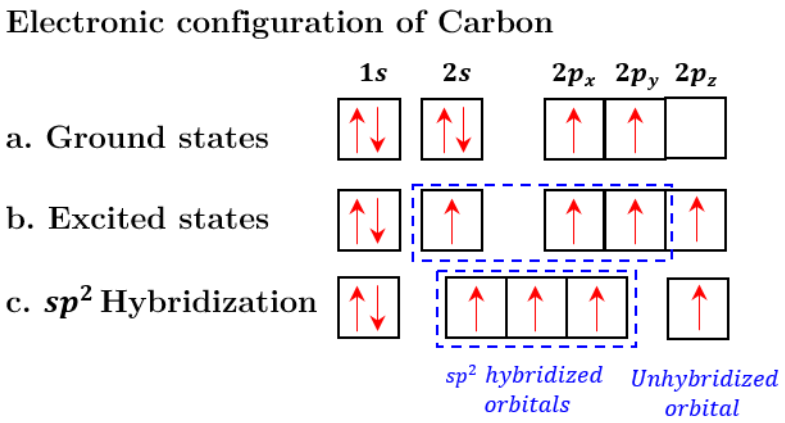

Figure 5 Electronic configuration of carbon a. In the ground state, $1s$ *and* $2s$ *subshells are completely filled and their electrons are not available for bonding. b. In the excited state, one of the electrons in the* $2s$ *subshell is promoted to* $2p$ *subshell, therefore we have four unpaired electrons i.e. one unpaired electron in each of the* $2s$, $2p_x$, $2p_y$ *and* $2p_z$ *orbitals. c.* sp^2 *hybridization occurs and the electrons in the orbitals* $2s$, $2p_x$, $2p_y$ *are involve.*

The sp^2 hybridized orbitals form strong σ—bonds in the plane of graphene with bond angles of 120°, and the remaining one electron in the 2pz orbitals forms the extended π—bond and it is able to participate with the free electrons from the other atoms. These π-bonds are responsible to give graphene the extraordinary electronic properties, such as electron transport [15].

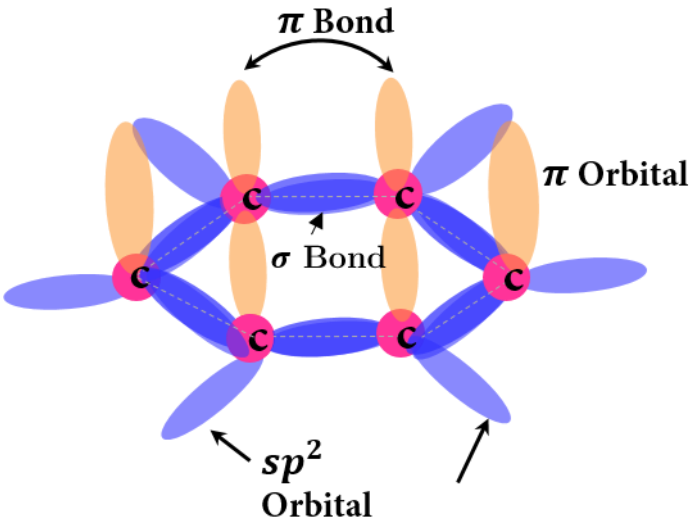

Figure 6 Molecular orbitals of graphene

On the other hand, when graphene is modified with functional groups such as hydroxyl, epoxyl, carbonyl and carboxyl groups (*see Figure 7*), the graphene oxide (GO) is obtained. There are various methods to synthetize GO, the Hummer method is usually employed. The presence of ionic groups such as O^- and COO^- in GO/rGO makes it possible to interact electrostatically with charged proteins or DNA, [4].

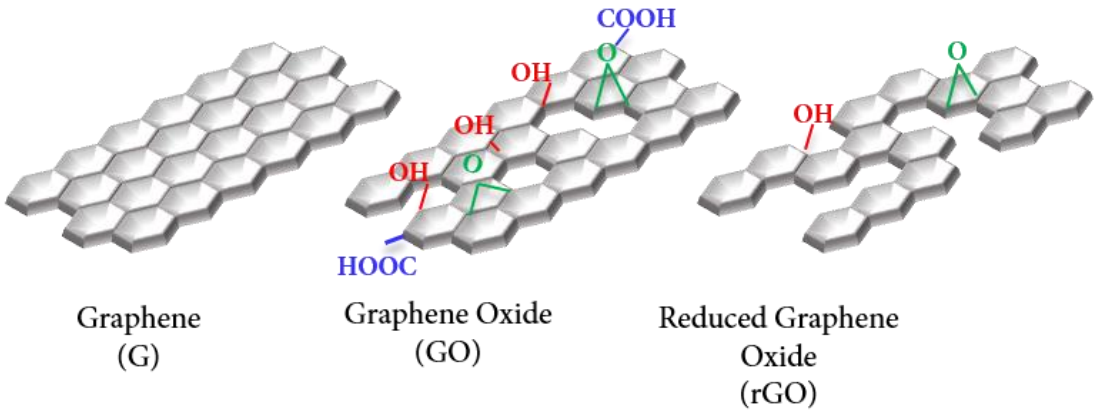

Figure 7 Structures of graphene, graphene oxide (GO) and reduced graphene oxide.

A great advantage of GO is the fact that we can control the oxidation level to optimize the optical, thermal or electrical properties, specifically, in solar cells, for example, different levels of oxidation have been studied to find the optimal relation C/O which indicates the number of oxygen atoms for each carbon atom, to enhance the power conversion efficiencies (PCE).[4] In optical biosensing, such as a FRET-based biosensing, there is a hypothesis which stablishes that reduced graphene oxide favors the analytical performance of a biosensing system, so the possibility to use reduced GO as acceptor in this type of biosensor must be considered [16].

Additionally, the oxidation level can be reflected in the band gap between the lowest unoccupied molecular orbital (LUMO) and the highest occupied molecular orbital (HOMO) as shown in Figure 8. The dispersed oxygen functional groups of GO make it an electronic insulator, while the absences of these groups in G make it a high charge mobility material. [17]

To shed light on the lattice as well as electronic band structure of graphene, GO and rGO, it is necessary to understand how the transformation of GO to rGO leads to high photoexcitation response.

The ordered hexagonal lattice of graphene becomes disordered by oxygen defects produced during chemical oxidization process.

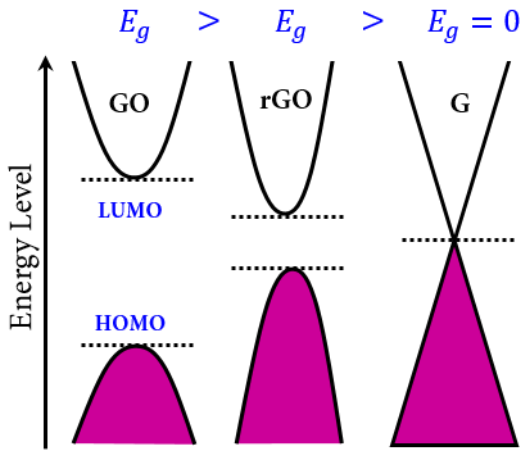

Figure 8 Electronic band structure of GO, rGO and G respectively. Essentially, the band gap represents the minimum energy that is required to excite an electron from the valence band to the conduction band, in organic materials, HOMO (highest occupied molecular orbital) and LUMO (lowest un-occupied molecular orbital), respectively. Graphene normally has a band gap of zero, however, oxygenation processes can modulate the width of this energy gap.

The quantity of disorder-induced states declines after reduction owing to deoxygenation. This structural modification is attributed to the reduction of oxygen functional groups and gradual recovery of the conjugations between carbon atoms during the reduction process. The reduction process leads to increased charge carrier mobility, higher absorption, a tunable bandgap where photo responsivity can be controlled by controlling the defects and oxygen groups. [18, 19, 20]

Characterization techniques

As previously mentioned, graphene and its derivatives have a wide variety of properties that can be used for the development of new applications, therefore, it is imperative to have techniques to identify them. Some of the most used techniques are:

- **Scanning electron microscopy (SEM):** This technique has a higher resolution than the optical microscope, since it works with a beam of focused electrons that interact with the atoms in the sample. To take a conventional SEM image, the sample is required to be conductive at least on the surface. The fundamental objective of this technique is to obtain a clear image of the thin film of the 2D materials. [21]

- **X-ray photoelectron spectroscopy (XPS)** This method is used to determine and study the chemical components of surfaces, especially to characterize the concentration and link it to dopant heteroatoms such as oxygen. Graphene quality characterization is carried out by means of the elementary relationship between the weight percent of carbon and oxygen (C/O). GO is an electrical insulator and the C/O ratio oscillates around 2, after reduction processes the rGO becomes conductive, so the C/O ratio increases. [22]

- **Fourier Transform Infrared Spectroscopy (FTIR)** This technique uses the normal modes of vibrations to provide molecular information. It is more efficient for polar molecules in which the vibrational modes are antisymmetric. The vibrational modes of a molecule are unique, therefore, FTIR allows the identification of organic components and structures from their absorption of infrared radiation.

  FTIR allows monitoring the reduction process, showing the characteristic bands of the hybridizations and functional groups of oxygen that may be present in the

material. [23]

- **Raman spectroscopy** This technique is a non-invasive tool and it is highly sensitive to vibrations in the structure and intramolecular bonds. Raman spectroscopy is widely used to obtain structural information of carbon materials. Typically, graphene derivatives Raman spectra exhibit two main bands, D and G. The first one (D band), provides information on the structural defects of sp^2 carbon and is located at approximately 1350 cm^{-1}. On the other hand, the G band is directly related to the vibrational mode in the plane of the sp^2 system and it is generally located at 1587 cm^{-1}.

Using the ratio of peak intensities I_D/I_G, from Raman spectra, it is possible to characterize the level of disorder in graphene, thereby the level of reduction in graphene oxide. [21] [24]

1.3.Operating mechanism of FRET-GO/rGO based biosensor

Biosensors which work with the fluorescence quenching mechanism, are based on the phenomenon of FRET, herein, a donor and an acceptor group are involved, this effect is directly related to the bio-recognition process. This process occurs when the donor's emission spectrum overlaps with the absorption spectrum of the acceptor and the molecular orbitals are close enough to interact. In this type of biosensing mechanism, GO is the molecular acceptor and a molecular donor is any fluorophore that has the complementary spectral profile and orientation, FITC (fluorescein isothiocyanate) is usually employed.[25] Figure 9

shows the spectral overlapping between the absorbance spectra of three different types of GO and the FITC emission spectrum.

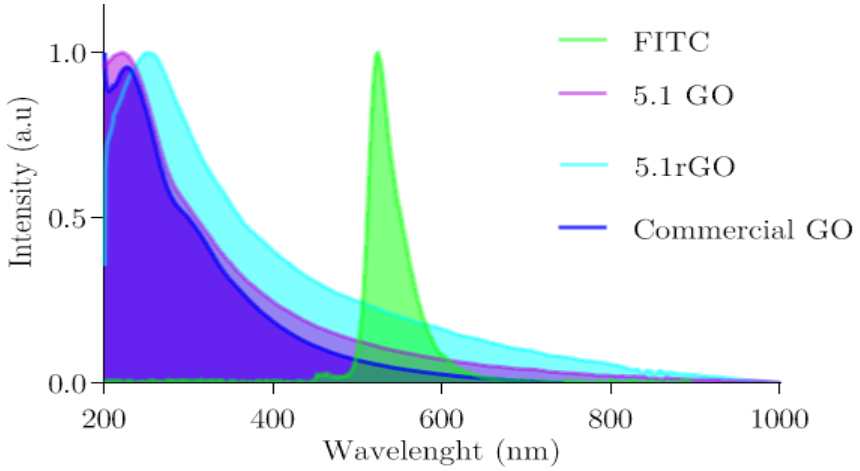

Figure 9 Spectral overlapping of the different graphene oxide samples and FITC molecule.

When biorecognition occurs (antibody-antigen association), changes in fluorescence intensities are generated, in other words, fluorescence quenching acts as a bio-recognition indicator. Hence, fluorescence quenching represents a powerful tool to get information in the biosensing field (Figure 10).

The operating mechanism of the biosensing platform is based on considering that in the absence of the analyte, a maximum fluorescence quenching will be experienced.

This quenching is due to the interaction between GO and the FITC fluorophore, such interaction is known as Förster resonance energy transfer (FRET), with FITC being the donor molecule and GO the acceptor molecule. This non-radiative energy transfer, increases over time due to increased interactions between fluorophore FITC and GO.

However, when the analyte is present, after a certain time, the fluorescence quenching will be proportional to the concentration of the analyte present. It can be considered that, the analyte acts as a "spacer" between the fluorophore and the GO, such that, the higher the concentration of the analyte the higher the number of analyte probe complexes; likewise, the higher the separation between the GO and the FITC.

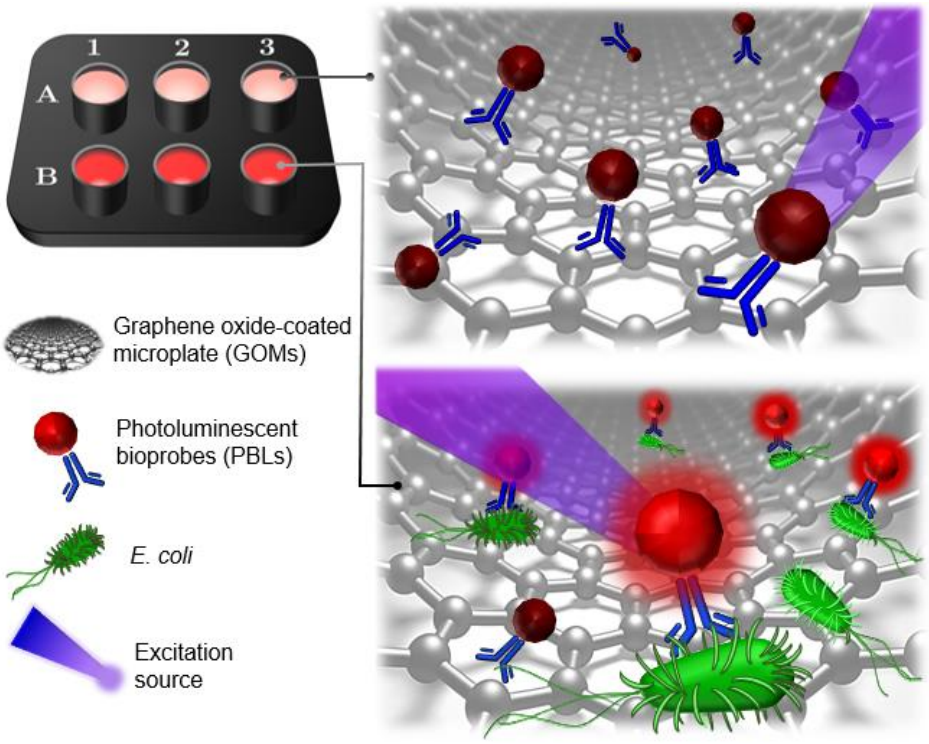

Figure 10 Operational principle of the proposed single-step, wash-free and real-time bacterial detection platform. Graphene oxide-coated microplates are conceived to deactivate the photoluminescence of those (Photoluminescent bioprobe) PLBs that are not undergoing immunoreactions via non-radiative energy transfer. Adapted with permission from 27, Copyright © 2020, American Chemical Society.

REFERENCES

(1) Morales-Narváez, E.; Merkoçi, A. Graphene Oxide as an Optical Biosensing Platform: A Progress Report. *Advanced Materials* **2019**, *31* (6), 1805043. https://doi.org/10.1002/adma.201805043.

(2) Morales, M. A.; Mark Halpern, J. Guide to Selecting a Biorecognition Element for Biosensors. *Bioconjug Chem* **2018**, *29* (10), 3231–3239. https://doi.org/10.1021/acs.bioconjchem.8b00592.

(3) Vessman, J.; Stefan, R. I.; Staden, J. F. V.; Danzer, K.; Lindner, W.; Burns, D. T.; Fajgelj, A.; Müller, H. Selectivity in Analytical Chemistry: (IUPAC Recommendations 2001). https://doi.org/10.1515/iupac.73.0808.

(4) Srivastava, S.; Senguttuvan, T. D.; Gupta, B. K. Highly Efficient Fluorescence Quenching with Chemically Exfoliated Reduced Graphene Oxide. *Journal of Vacuum Science & Technology B* **2018**, *36* (4), 04G104. https://doi.org/10.1116/1.5026170.

(5) Velasco-Soto, M. A.; Pérez-García, S. A.; Alvarez-Quintana, J.; Cao, Y.; Nyborg, L.; Licea-Jiménez, L. Selective Band Gap Manipulation of Graphene Oxide by Its Reduction with Mild Reagents. *Carbon* **2015**, *93*, 967–973. https://doi.org/10.1016/j.carbon.2015.06.013.

(6) Jameson, D. Introduction to Fluorescence: https://www.amazon.com.mx/Introduction-Fluorescence-David-M-Jameson/dp/1439806047 (accessed Jul 13, 2020).

(7) Bernard Valeur. Molecular Fluorescence: Principles and Applications, 2nd Edition | Wiley us/Molecular+Fluorescence%3A+Principles+and+Applications%2C+2nd+Edition-p-9783527328376 (accessed Jul 13, 2020).

(8) Forster, Th. Energiewanderung und Fluoreszenz. *Naturwissenschaften* **1946**, *33* (6), 166–175. https://doi.org/10.1007/BF00585226.

(9) Lakowicz, J. R. *Principles of Fluorescence Spectroscopy*, 3rd ed.; Springer US, 2006. https://doi.org/10.1007/978-0-387-46312-4.

(10) Tisler, J.; Oeckinghaus, T.; Stöhr, R. J.; Kolesov, R.; Reuter, R.; Reinhard, F.; Wrachtrup, J. Single Defect Center Scanning Near-Field Optical Microscopy on Graphene. *Nano Lett.* **2013**, *13* (7), 3152–3156. https://doi.org/10.1021/nl401129m.

(11) Arnault, J.-C. *Nanodiamonds: Advanced Material Analysis, Properties and Applications*; William Andrew, 2017.

(12) Hussain, S. A. An Introduction to Fluorescence Resonance Energy Transfer (FRET). *Energy* **2009**, *132*.

(13) Geim, A. K.; Novoselov, K. S. The Rise of Graphene. *Nature Materials* **2007**, *6* (3), 183–191. https://doi.org/10.1038/nmat1849.

(14) Lloyd-Hughes, J.; Jeon, T.-I. A Review of the Terahertz Conductivity of Bulk and Nano-

Materials. *J Infrared Milli Terahz Waves* **2012**, *33*, 871. https://doi.org/10.1007/s10762-012-9905-y.

(15) Wallace, P. R. The Band Theory of Graphite. *Phys. Rev.* **1947**, *71* (9), 622–634. https://doi.org/10.1103/PhysRev.71.622.

(16) Yu, H.; Zhang, B.; Bulin, C.; Li, R.; Xing, R. High-Efficient Synthesis of Graphene Oxide Based on Improved Hummers Method. *Scientific Reports* **2016**, *6* (1), 36143. https://doi.org/10.1038/srep36143.

(17) Sapsford, K. E.; Berti, L.; Medintz, I. L. Materials for Fluorescence Resonance Energy Transfer Analysis: Beyond Traditional Donor-Acceptor Combinations. *Angew. Chem. Int. Ed. Engl.* **2006**, *45* (28), 4562–4589. https://doi.org/10.1002/anie.200503873.

(18) Jin, Y.; Zheng, Y.; Podkolzin, S. G.; Lee, W. Band Gap of Reduced Graphene Oxide Tuned by Controlling Functional Groups. *J. Mater. Chem. C* **2020**, *8* (14), 4885–4894. https://doi.org/10.1039/C9TC07063J.

(19) Loh, K. P.; Bao, Q.; Eda, G.; Chhowalla, M. Graphene Oxide as a Chemically Tunable Platform for Optical Applications. *Nat Chem* **2010**, *2* (12), 1015–1024. https://doi.org/10.1038/nchem.907.

(20) Chien, C.-T.; Li, S.-S.; Lai, W.-J.; Yeh, Y.-C.; Chen, H.-A.; Chen, I.-S.; Chen, L.-C.; Chen, K.-H.; Nemoto, T.; Isoda, S.; Chen, M.; Fujita, T.; Eda, G.; Yamaguchi, H.; Chhowalla, M.; Chen, C.-W. Tunable Photoluminescence from Graphene Oxide. *Angew. Chem. Int. Ed. Engl.* **2012**, *51* (27), 6662–6666. https://doi.org/10.1002/anie.201200474.

(21) Abid; Sehrawat, P.; Islam, S. S.; Mishra, P.; Ahmad, S. Reduced Graphene Oxide (RGO) Based Wideband Optical Sensor and the Role of Temperature, Defect States and Quantum Efficiency. *Sci Rep* **2018**, *8* (1), 3537. https://doi.org/10.1038/s41598-018-21686-2.

(22) Hu, M.; Yao, Z.; Wang, X.; Department of Chemical, Biological and Pharmaceutical Engineering, New Jersey Institute of Technology, Newark, NJ 07102, USA. Characterization Techniques for Graphene-Based Materials in Catalysis. *AIMS Materials Science* **2017**, *4* (3), 755–788. https://doi.org/10.3934/matersci.2017.3.755.

(23) XPS Interpretation of Carbon https://xpssimplified.com/elements/carbon.php (accessed Jul 28, 2020).

(24) FTIR Spectroscopy - an overview | ScienceDirect Topics https://www.sciencedirect.com/topics/earth-and-planetary-sciences/ftir-spectroscopy (accessed Jul 28, 2020).

(25) Jaureguib, L. A.; Parkb, W.; Caoa, H.; Chena, Y. P.; Childres, I.; Jauregui, L. A.; Park, W.; Al, E. *Raman Spectroscopy of Graphene and Related Materials*.

(26) Huang, A.; Li, W.; Shi, S.; Yao, T. Quantitative Fluorescence Quenching on Antibody-Conjugated Graphene Oxide as a Platform for Protein Sensing. *Scientific Reports* **2017**, *7* (1), 40772. https://doi.org/10.1038/srep40772.

CHAPTER 2.

GO PROPERTIES AND ITS ROLE IN THE OPTICAL BIOSENSING FIELD: STATE OF THE ART

Currently, optical biosensing systems have become a fundamental tool in the development of studies related to health care, analysis of food, safety and protection as well as environmental monitoring, among others. Hence, highly sensitive systems are crucial in this field. [26]

Since, Andre Geim and Konstantin Novoselov earned the Nobel Prize in Physics, in 2010, due their theoretical contributions to the understanding of graphene, the interest of the scientific community towards this material has increased remarkably. [27]

An interesting fact about graphene and its derivatives in general, is that their properties can be enhanced according to the requirements of a given application. This makes graphene and its derivatives versatile and potentially useful materials in biosensing as well as other scientific fields. [28]

One of the ways in which the properties of graphene can be modified is mainly through three structural parameters, its lateral size, number of layers and degrees of oxidation.

Some studies have revealed that the optical properties of GO, such as, optical transmittance can be controlled according to the number of layers or just applying an external electric field on a monolayer.[29] [30] [31] Which might be useful to develop biosensors

based on electrochromic or optoelectronic mechanisms. [32] [33]

Additionally, studies have shown that the modulation of fluorescence is related with number of GO layers, however, the results obtained by the researchers contradict each other, whereas one investigation performed in 2010 indicates that the quenching efficiency increases with layer numbers, [34] other experiment carried out in 2013, states that the quenching factor decreases from monolayer to 2–4 layers graphene. [35] Until now, is not possible to establish a clear relationship between the modulation of fluorescence quenching and the number of layers of the GO.

Furthermore, the lateral size of the GO is an important structural parameter in the development of biosensing platforms. Studies have presented experimental evidence that GO flakes with a certain lateral size can be more or less efficient as fluorescence quenchers [36] Additionally, from a study on the interaction of DNA and GO with different lateral sizes, it was concluded that DNA presented a better adsorption for GO with lateral size of the order of nm than μm, this is a useful parameter for the design of biosensing platforms which require a quick response. [37]

In the design of biosensors, the study between the interaction of GO and cells, pathogens and other biological elements is very important since it is of great relevance for biomedical applications (therapy, bioimaging, drug administration).

In addition, the oxidation degree of GO, can be modulated by different chemical methods that provide GO samples with different structural features resposables of new properties. Some studies have revealed that distribution of functional groups of oxygen is directly related to the physicochemical properties, [38,39] for example, photoluminescent emission, [40] [41] thermal conductivity, [42] fluorescence quenching ability, [43] among other properties of GO

Modulation of photoluminescence quenching through oxidation levels requires extensive

work, since parameters such as the number of layers and the lateral size must be controlled.

2.1. Biosensors with FRET approach

One of the most promising properties of GO and of particular relevance to the development of this thesis is the photoluminescence quenching, [44] many researchers are taking advantage of this effect to developed biosensors using the fluorescence quenching approach. [45] [46]

As already mentioned, functional groups on the surface and edge of GO have an important role in fluorescence quenching of a fluorophore. [47] The scientific community has been working a lot to find the advantages of reduced graphene oxide in several applications. A study performed in 2017 has shown that after reduction process the quenching efficiency of GO increases significantly.

So the hypothesis that reduced graphene oxide favors the analytical performance of a biosensing system by means of a more efficient quenching of fluorescence, is supported by this literature.

Commonly, protein detection has been one of the applications of FRET-based biosensors, requiring for this an acceptor donor pair.[48,49]

Since FRET generates a real-time fluorescent signal that changes spatially and temporally with the distribution of the fluorescent substance, it has served as a strategy in the design of different biosensors for disease diagnosis, drug detection and other biological applications. [45,46,50–52] Figure 10 shows some GO-based biosensors with fluorescence quenching approach. Additionally, the most relevant aspects of these and some of G/GO-based biosensors found in the literature are summarized in Table 1.

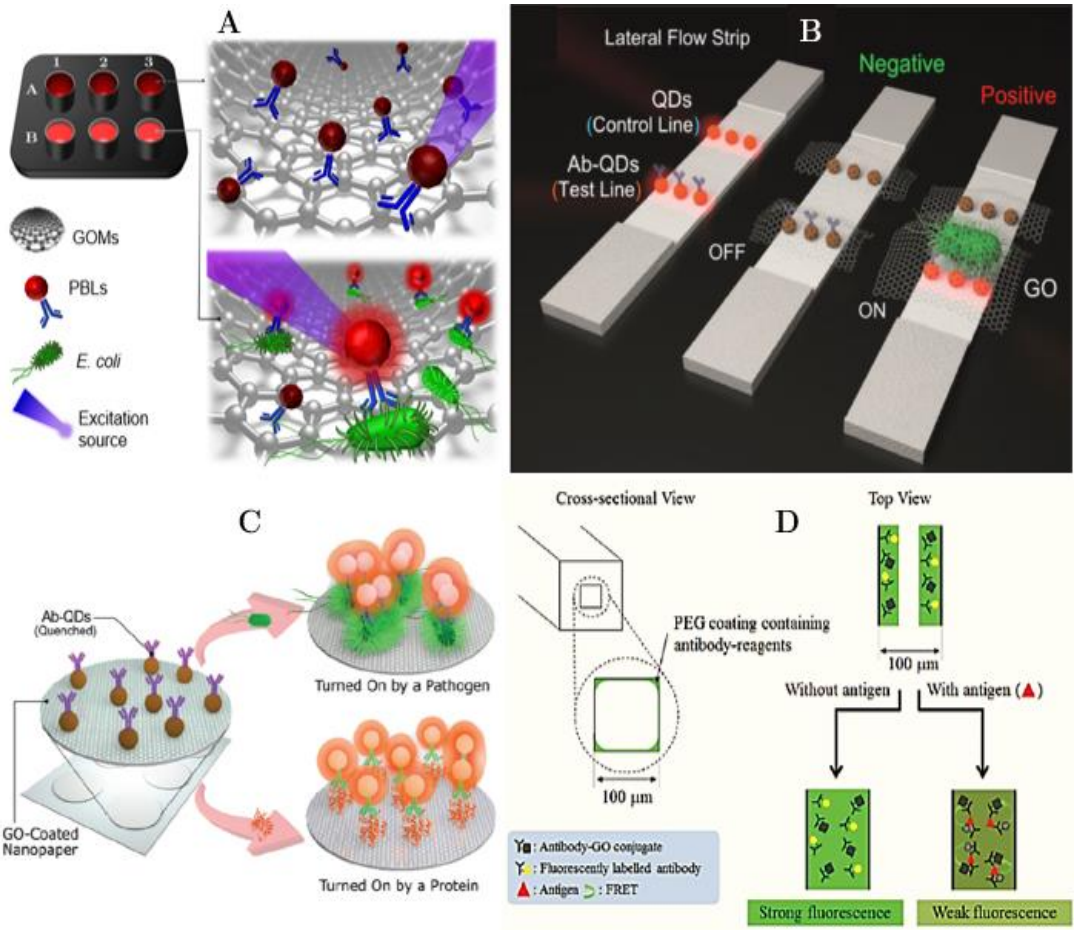

Figure 11 Some biosensor with FRET approach A. Operational principle of the proposed single-step, wash-free and real-time bacterial detection platform. Adapted with permission from [45], Copyright © 2020 American Chemical Society. B. Lateral flow device based on NRET for pathogen detection. Adapted with permission from [53] Copyright 2015, American Chemical Society. C. GO-coated Nano paper immunosensing platform for protein detection. Adapted with permission from [54] Copyright © 2017, Wiley-VCH. D. Biosensor consisting of a polyethylene glycol (PEG) coating containing two types of antibody. One conjugated with GO and the second conjugated with a fluorophore. Adapted with permission from [55] Copyright © 2016, RSC.

Table 1. GO-based biosensors with fluorescence quenching approach.

Graphene type	Highlighted properties	Analyte	Detection limit	Year	Ref
Graphene Oxide (GO)	Single-step, wash-free, and real-time bacterial detection platform	Escherichia Coli bacteria	2 CFU mL^{-1}	2020	[45]
Graphene Oxide (GO)	Quick and virtually universal single-step immunosensing	Human –IgG/ Prostate specific	0.02 - 2.56 µg mL^{-1}	2020	[46]

Graphene type	Highlighted properties	Analyte	Detection limit	Year	Ref
	platform is reported.	antigen (PSA)			
Graphene Oxide (GO)	Device low cost and easy use.	Human immunoglobulin G (IgG)	1.35 ng mL^{-1} in standard buffer and 6.36 ng mL− 1 in human serum	2018	[53]
Graphene Oxide (GO)	Using a single antibody and without the need for washing steps	Human immunoglobulin G (IgG) and The Escherichia Coli bacteria	55 CFU mL^{-1} for the bacterium and 1.91 ng mL^{-1} for the immunoglobulin	2017	[56]
Graphene Oxide (GO)	High FRET efficiency (90% approx.) .	Human immunoglobulin M (IgM)	0.29 µg mL^{-1}	2016	[55]
Graphene Oxide (GO)	Avoid the secondary antibodies.	Escherichia Coli bacteria	10 CFU mL^{-1} in standard buffer and 100 CFU mL^{-1} in bottled water and milk	2015	[57]
functionalized graphene with Carboxyl residues	Multiple analyte detection.	Chicken and mouse immunoglobulin	In the nanomolar range	2014	[58]
Colloidal Graphene	Reduces detection time by less than 35 minutes	MC-LR	0.14 µg mL^{-1}	2012	[59]

In most of the articles, the important characteristic of this material to improve the sensitivity in biosensing system is highlighted due to its electrical conductivity, high rate of electron transfer, ability to quenching photoluminescence and its high charge capacity, as well as to immobilize enzymes. According to literature, GO has been employed in general as a signal amplifier material or as an energy acceptor material.

In this thesis, specifically, we will take advantage of the ability of GO as a fluorescence quencher through FRET phenomenon. We pretend optimize the FRET phenomenon through reducing GO and thus develop a more sensitive and efficient biosensing platform.

REFERENCES

(27) Damborský, P.; Švitel, J.; Katrlík, J. Optical Biosensors. *Essays Biochem.* **2016**, *60* (1), 91–100. https://doi.org/10.1042/EBC20150010.

(28) The Nobel Prize in Physics 2010 https://www.nobelprize.org/prizes/physics/2010/press-release/ (accessed Aug 3, 2020).

(29) Wypych, G. Graphene: Important Results and Applications; Elsevier, 2019. https://www.elsevier.com/books/graphene/wypych/978-1-927885-51-2

(30) Goumri, M.; Lucas, B.; Ratier, B.; Baitoul, M. Electrical and Optical Properties of Reduced Graphene Oxide and Multi-Walled Carbon Nanotubes Based Nanocomposites: A Comparative Study. Optical Materials 2016, 60, 105–113. https://doi.org/10.1016/j.optmat.2016.07.010.

(31) Joung, D.; Gu, T.; Cho, J.-H. Tunable Optical Transparency in Self-Assembled Three-Dimensional Polyhedral Graphene Oxide. *ACS Nano* **2016**, *10* (10), 9586–9594. https://doi.org/10.1021/acsnano.6b04971.

(32) Qiao, Z.; Qin, C.; Gao, Y.; Zhang, G.; Chen, R.; Xiao, L.; Jia, S. Modulation of the Optical Transmittance in Monolayer Graphene Oxide by Using External Electric Field. *Scientific Reports* **2015**, *5* (1), 14441. https://doi.org/10.1038/srep14441.

(33) Lu, C.; Huang, P.-J. J.; Liu, B.; Ying, Y.; Liu, J. Comparison of Graphene Oxide and Reduced Graphene Oxide for DNA Adsorption and Sensing. *Langmuir* **2016**, *32* (41), 10776–10783. https://doi.org/10.1021/acs.langmuir.6b03032.

(34) Tong, L.; Qi, W.; Wang, M.; Huang, R.; Su, R.; He, Z. Tunable Design of Structural Colors Produced by Pseudo-1D Photonic Crystals of Graphene Oxide. *Small* **2016**, *12* (25), 3433–3443. https://doi.org/10.1002/smll.201600148.

(35) Chen, Z.; Berciaud, S.; Nuckolls, C.; Heinz, T. F.; Brus, L. E. Energy Transfer from Individual Semiconductor Nanocrystals to Graphene. *ACS Nano* **2010**, *4* (5), 2964–2968. https://doi.org/10.1021/nn1005107.

(36) Guo, X. T.; Hua Ni, Z.; Yan Liao, C.; Yan Nan, H.; Zhang, Y.; Wei Zhao, W.; Hui Wang, W. Fluorescence Quenching of CdSe Quantum Dots on Graphene. *Appl. Phys. Lett.* **2013**, *103* (20), 201909. https://doi.org/10.1063/1.4831670.

(37) Zhang, H.; Jia, S.; Lv, M.; Shi, J.; Zuo, X.; Su, S.; Wang, L.; Huang, W.; Fan, C.; Huang, Q. Size-Dependent Programming of the Dynamic Range of Graphene Oxide–DNA Interaction-Based Ion Sensors. *Anal. Chem.* **2014**, *86* (8), 4047–4051. https://doi.org/10.1021/ac500627r.

(38) Wang, J.; Quershi, W. A.; Li, Y.; Xu, J.; Nie, G. Analytical Methods for Nano-Bio Interface Interactions. *Sci. China Chem.* **2016**, *59* (11), 1467–1478. https://doi.org/10.1007/s11426-016-0340-1.

(39) Kiang Chua, C.; Pumera, M. Chemical Reduction of Graphene Oxide: A Synthetic Chemistry Viewpoint. *Chemical Society Reviews* **2014**, *43* (1), 291–312. https://doi.org/10.1039/C3CS60303B.

(40) Kumar, P. V.; Bardhan, N. M.; Chen, G.-Y.; Li, Z.; Belcher, A. M.; Grossman, J. C. New Insights into the Thermal Reduction of Graphene Oxide: Impact of Oxygen Clustering. *Carbon* **2016**, *100*, 90–98. https://doi.org/10.1016/j.carbon.2015.12.087.

(41) Zhang, F.; Liu, F.; Wang, C.; Xin, X.; Liu, J.; Guo, S.; Zhang, J. Effect of Lateral Size of Graphene Quantum Dots on Their Properties and Application. *ACS Appl. Mater. Interfaces* **2016**, *8* (3), 2104–2110. https://doi.org/10.1021/acsami.5b10602.

(42) Maiti, R.; Midya, A.; Narayana, C.; Ray, S. K. Tunable Optical Properties of Graphene Oxide by Tailoring the Oxygen Functionalities Using Infrared Irradiation. *Nanotechnology* **2014**, *25* (49), 495704. https://doi.org/10.1088/0957-4484/25/49/495704.

(43) Mu, X.; Wu, X.; Zhang, T.; Go, D. B.; Luo, T. Thermal Transport in Graphene Oxide – From Ballistic Extreme to Amorphous Limit. *Scientific Reports* **2014**, *4* (1), 3909. https://doi.org/10.1038/srep03909.

(44) Hong, B. J.; An, Z.; Compton, O. C.; Nguyen, S. T. Tunable Biomolecular Interaction and Fluorescence Quenching Ability of Graphene Oxide: Application to "Turn-on" DNA Sensing in Biological Media. *Small* **2012**, *8* (16), 2469–2476. https://doi.org/10.1002/smll.201200264.

(45) Real-Time Photoluminescent Biosensing Based on Graphene Oxide-Coated Microplates: A Rapid Pathogen Detection Platform | Analytical Chemistry https://pubs.acs.org/doi/abs/10.1021/acs.analchem.0c02200 (accessed Jul 20, 2020).

(46) Ortiz-Riaño, E. J.; Avila-Huerta, M. D.; Mancera-Zapata, D. L.; Morales-Narváez, E. Microwell Plates Coated with Graphene Oxide Enable Advantageous Real-Time Immunosensing Platform. *Biosensors and Bioelectronics* **2020**, *165*, 112319. https://doi.org/10.1016/j.bios.2020.112319.

(47) Chawjiraphan, W.; Apiwat, C.; Segkhoonthod, K.; Treerattrakoon, K.; Pinpradup, P.; Sathirapongsasuti, N.; Pongprayoon, P.; Luksirikul, P.; Isarankura-Na-Ayudhya, P.; Japrung, D. Sensitive Detection of Albuminuria by Graphene Oxide-Mediated Fluorescence Quenching Aptasensor. *Spectrochimica Acta Part A: Molecular and Biomolecular Spectroscopy* **2020**, *231*, 118128. https://doi.org/10.1016/j.saa.2020.118128.

(48) Frommer, W.; Davidson, M.; Campbell, R. ChemInform Abstract: Genetically Encoded Biosensors Based on Engineered Fluorescent Proteins. *Cheminform* **2009**, *40*. https://doi.org/10.1002/chin.200951271.

(49) Mertens, H. D. T.; Piljić, A.; Schultz, C.; Svergun, D. I. Conformational Analysis of a Genetically Encoded FRET Biosensor by SAXS. *Biophys J* **2012**, *102* (12), 2866–2875. https://doi.org/10.1016/j.bpj.2012.05.009.

(50) Zhang, X.; Xiao, Y.; Qian, X. A Ratiometric Fluorescent Probe Based on FRET for Imaging Hg2+ Ions in Living Cells. *Angew. Chem. Int. Ed. Engl.* **2008**, *47* (42), 8025–8029. https://doi.org/10.1002/anie.200803246.

(51) Wu, C.; Zhou, Y.; Miao, X.; Ling, L. A Novel Fluorescent Biosensor for Sequence-Specific Recognition of Double-Stranded DNA with the Platform of Graphene Oxide. *Analyst* **2011**, *136* (10), 2106–2110. https://doi.org/10.1039/C1AN15061H.

(52) Hu, B.; Hu, L.-L.; Chen, M.-L.; Wang, J.-H. A FRET Ratiometric Fluorescence Sensing System for Mercury Detection and Intracellular Colorimetric Imaging in Live Hela Cells. *Biosensors and Bioelectronics* **2013**, *49*, 499–505. https://doi.org/10.1016/j.bios.2013.06.004.

(53) Zamora-Gálvez, A.; Morales-Narváez, E.; Romero, J.; Merkoçi, A. Photoluminescent Lateral Flow Based on Non-Radiative Energy Transfer for Protein Detection in Human Serum. *Biosensors and Bioelectronics* **2018**, *100*, 208–213. https://doi.org/10.1016/j.bios.2017.09.013.

(54) Cheeveewattanagul, N.; Morales-Narváez, E.; Hassan, A.-R. H. A.; Bergua, J. F.; Surareungchai, W.; Somasundrum, M.; Merkoçi, A. Straightforward Immunosensing Platform Based on Graphene Oxide-Decorated Nanopaper: A Highly Sensitive and Fast Biosensing Approach. *Advanced Functional Materials* **2017**, *27* (38), 1702741. https://doi.org/10.1002/adfm.201702741.

(55) Shirai, A.; Henares, T. G.; Sueyoshi, K.; Endo, T.; Hisamoto, H. Fast and Single-Step Immunoassay Based on Fluorescence Quenching within a Square Glass Capillary Immobilizing Graphene Oxide–Antibody Conjugate and Fluorescently Labelled Antibody. *Analyst* **2016**, *141* (11), 3389–3394. https://doi.org/10.1039/C5AN02637G.

(56) Shirai, A.; Nakashima, K.; Sueyoshi, K.; Endo, T.; Hisamoto, H. Development of a Single-Step Immunoassay Microdevice Based on a Graphene Oxide-Containing Hydrogel Possessing Fluorescence Quenching and Size Separation Functions. *Analyst* **2017**, *142* (3), 472–477. https://doi.org/10.1039/C6AN02485H.

(57) Morales-Narváez, E.; Golmohammadi, H.; Naghdi, T.; Yousefi, H.; Kostiv, U.; Horák, D.; Pourreza, N.; Merkoçi, A. Nanopaper as an Optical Sensing Platform. *ACS Nano* **2015**, *9* (7), 7296–7305. https://doi.org/10.1021/acsnano.5b03097.

(58) Anfossi, L.; Calza, P.; Sordello, F.; Giovannoli, C.; Di Nardo, F.; Passini, C.; Cerruti, M.; Goryacheva, I. Y.; Speranskaya, E. S.; Baggiani, C. Multi-Analyte Homogenous Immunoassay Based on Quenching of Quantum Dots by Functionalized Graphene. *Anal Bioanal Chem* **2014**, *406* (20), 4841–4849. https://doi.org/10.1007/s00216-014-7885-6.

(59) Colloidal Graphene as a Transducer in Homogeneous Fluorescence-Based Immunosensor for Rapid and Sensitive Analysis of Microcystin-LR | Environmental Science & Technology

CHAPTER 3.

EXPERIMENTAL METHODS

In order to achieve the objectives, set for this thesis, fluorescence quenching analyses were performed on GO/rGO based-biosensing platforms. Principally, different types of GO/rGO were employed as well as different concentrations of GO/rGO and IgG-FITC.

Previous to the kinetic fluorescence quenching analyses, studies such as GO adhesion on microplate surfaces and characterization of the reduction process were performed and will be described with more detail below. Importantly, this series of experiments is reported in the article "Microwell plates coated with graphene oxide enable advantageous real-time immunosensing platform", Biosensors and Bioelectronics, 2020, 112319. [46]

3.1.Reagents and Equipment.

- Monolayer GO aqueous suspension was acquired from Angstron Materials (OH, USA), lateral size around 500 nm, carbon/oxygen ratio around 1.
- GO and rGO aqueous suspension synthetized by Laboratorio de Catálisis CFATA research group, lateral size around 500 nm for GO and 220 nm for rGO. Carbon/oxygen ratio for rGO 30:1.
- Amino-functionalized 96 well black plates with bottom and lid of polystyrene were purchased from Corning Inc. (Corning, NY, USA), (TCT microplates).[60]
- High binding 96 well plates with bottom and lid of polystyrene were purchased from

Corning Inc. (Corning, NY, USA). (HB microplates). [61]

- Polyclonal anti-HIgG-FITC was purchased from Abcam (Cambridge, UK).
- Phosphate buffered saline (PBS) tablets were purchased from Sigma-Aldrich (San Luis, MI, USA).
- L-AAscorbic acid (L-AA) was acquired from Sigma-Aldrich (Toluca, Mexico, Mexico).
- Poly-L-Lysine coated glass slides were purchased from Polysciences Europe GmbH (Hirschberg an der Bergstrasse, Germany).
- All aqueous solutions were freshly prepared in ultrapure water, Milli-Q system (>18.2 MΩ cm−1, Millipore).
- Photoluminescence experiments were performed in a Cytation 5 multi-mode reader (BioTek, Winooski, VT, U.S.A.)
- Raman spectra were recorded via Renishaw in Via Raman module for spectroscopic analysis (Wotton-under-Edge, UK), which is coupled on a Leica DM 2500M microscope in vertical configuration. A 50× objective (NA = 0.75) and blue excitation line (457 nm) were employed in all experiments.

3.2.Characterization of GO adhesion

In this stage, the quantity of GO which remains adhered to microplates surface was estimated. This information is relevant because it is associated with the amount of reducing agent, L-AA (L-Ascorbic acid) required to begin the reduction process.

3.2.1. TCT plate and Poly-L-Lysine glass slide coating with GO

The first step was to prepare GO suspensions with concentrations of 300, 600, 1200, 1400 and 1600 μgmL^{-1}. These suspensions were deposited on poly-L-lysine coated glass slides, as

shown in Figure 12a. Moreover, GO suspensions concentrated at 1200, 1400 and 1600 μg/mL were deposited within microwells formed with a silicone mask using poly-L-lysine coated glass slides as a surface, according to the Figure 12b. These samples were incubated during 24 hours approximately. Washing were performed by adding and extracting 100 μL of ultrapure water (usually three times) to remove excess of GO, which was not adhered to the surface.

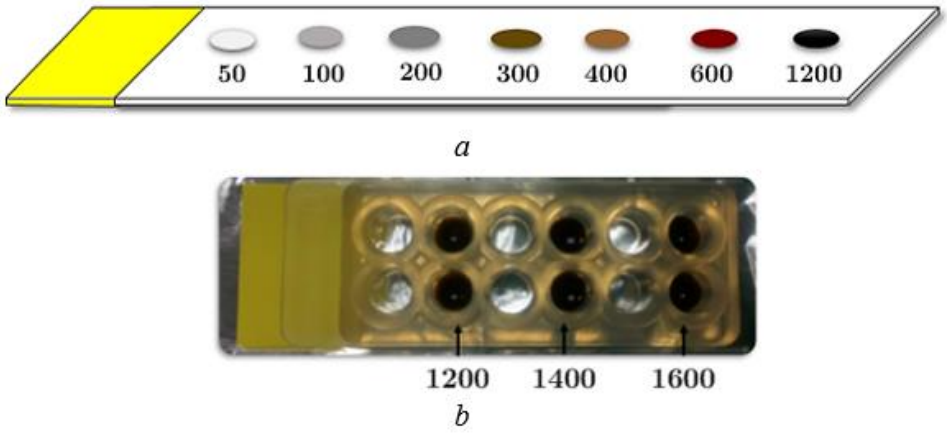

Figure 12 GO suspensions ***a.*** *GO suspensions on Poly-L-Lysine coated glass slides.* ***b.*** *GO suspensions in a silicone mask.*

According to previous studies, [46] polystyrene produces relatively strong scattering compared with the scattering produced by the low concentration of GO deposited onto microplates, which does not allow to observe the Raman signal of GO adhered on the surface. In order to avoid the polystyrene scattering, the experiment was transferred in poly-L-lysine coated glass slides.

3.2.2. Raman spectra analysis.

Herein, 10 spectral measurements were made for corresponding drop of GO concentration (50, 100, 200, 300, 400, 600, 1200 μg mL^{-1}). The spectral information was obtained once the drops had dried at room temperature onto poly-L-lysine slides.

To estimate the amount of GO adhered on the surface, it was necessary to make a calibration curve based on the results of Raman scattering intensity at D an G peaks.

Other poly-l-lysine glass slides were masked with microwell-like silicone gaskets and incubated with GO at 1200 and 1600 μg mL^{-1} in order to produce GO microwell plates (as described above) onto these glass slides coated with amino groups.

The Raman signature of these samples were also analyzed to perform an interpolation within the resulting calibration curve, particularly using the resulting Raman scattering intensity at D and G peaks.

3.3.Characterization of reduction process

Before starting the reduction process, it was necessary to have a TCT plate coated with GO, a silicone mask and a poly-L-lysine coated glass slide.

TCT plate and poly-L-lysine glass slide coating with GO:

To carry out TCT plate coating, 100 μL of GO suspension were adhered in each well of the plate, in particular, 1 to 6 columns, B, C and D rows were coated with 1200, 1600 and 2000 μg mL^{-1} respectively. After that, the plate is subjected to 600 rpm stirring during 12 hours. Once past this period, three washing stages were made with ultrapure water.

The same way to the process of GO adhesion described above, silicone mask and Poly-L-Lysine coated glass slide was employed to the incubation process according to the Figure

12b.

Reduction process

To perform the reduction process of the GO via L-ascorbic acid (L-AA), 50 mg of L-AA were added to 50 mL of ultrapure water. For 40 minutes the mixture remained under vigorous stirring and 90 ° C. The concentration of a resultant aqueous dilution was 1000 μg mL^{-1}.

Herein, we used the L-AA concentration recommended and protocol of reduction by Jiali Zhang *e tal* , [62] which indicates that the amount of L-AA to be used should be 3.5 times the concentration of GO (3.5×[GO]), in addition, we also decided to use half of this amount according to the table 2 and 3.

Table 2.Conditions for the reduction process

Experiment	[LAA] (μg mL-1)	Time	Temperature (°C)
1	1.75 ×[GO]	40 min	90
2		48 h	Room temperature
3	3.5 ×[GO]	40 min	90
4		48 h	Room temperature

Note: During the reduction process the samples were under constant stirring at 350 rpm in all experiments.

Table 3.Amount of [L-AA] in function of [GO] adhered

Initial [GO, μg mL^{-1}]	Adhered [GO, μg mL^{-1}]	[L-AA, μg mL^{-1}] required to reduction	
		1.75 x [GO]	3.5 x [GO]
1200	60	105	210
1600	80	140	280
2000	100	175	350

To obtain the required [L-AA] shown in Table 4, the following mathematical expression is used:

$$C_i.V_i = C_f.V_f \qquad (4)$$

This expression relates the final and initial volumes and concentrations in the process of preparing an aqueous dilution. Table 4 and 5 show that the quantities extracted from the first dilution of L-AA (1000 µg mL-1) and ultrapure water, in order to obtain the required concentrations.

Table 4. Quantities of L-AA and ultrapure to 1.75×[GO] reduction

[L-AA, µg mL-1] required	L-AA (µL)	Ultrapure water (µL)
105	126	1074
140	168	1032
175	210	990

Table 5. Quantities of L-AA an ultrapure to 3.5×[GO] reduction

[L-AA, µg mL^{-1}] required	L-AA (µL)	Ultrapure water (µL)
210	252	948
280	336	864
350	420	780

Note: Each of the prepared solutions has a total volume of 1200 µL.

Once the diluted solutions for 1.75×[GO] and 3.5×[GO] reduction have been prepared, 200 µL of each solution are added per well of a TCT plate as shown in the Figure 13.

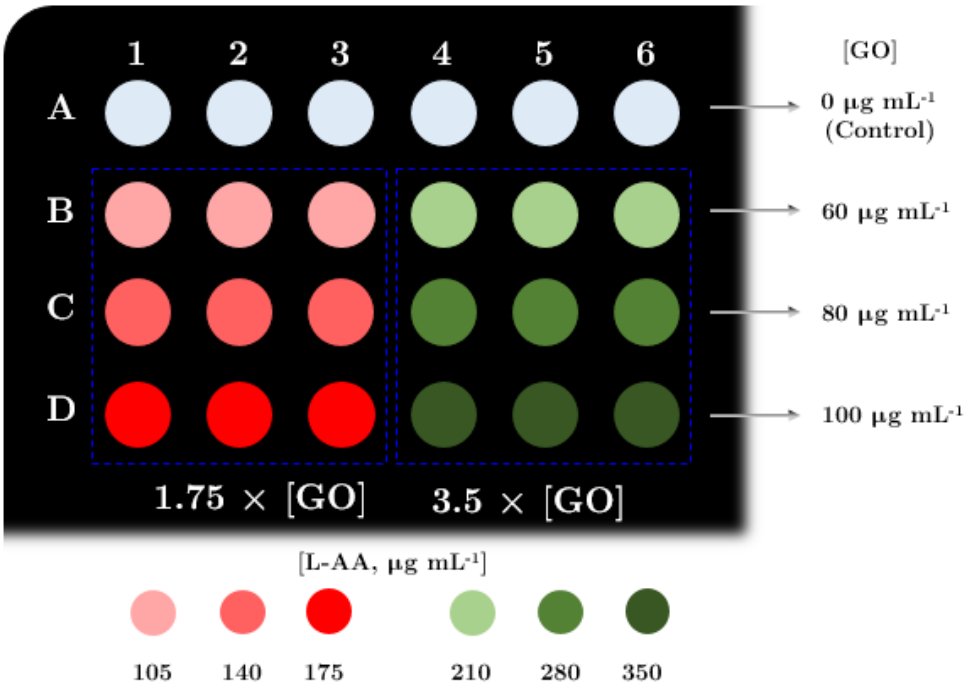

Figure 13 L-AA addition representation in well plates.

In a similar way, 200 µL of each solution are added per well of a silicone mask (see Figure 14).

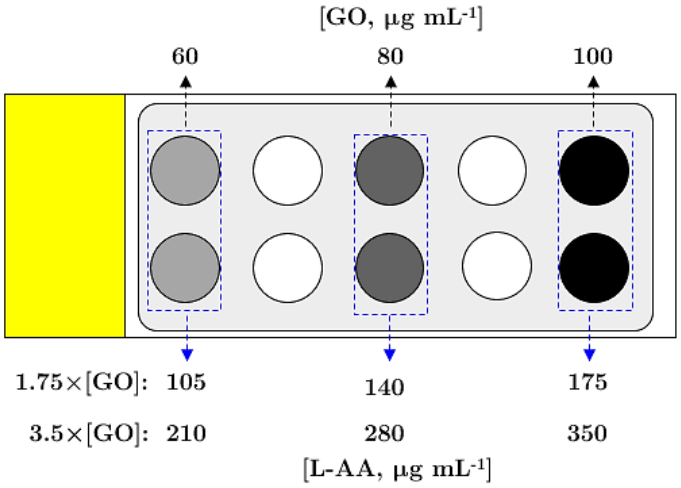

Figure 14 L-AA addition scheme in Poly-L-Lysine coated glass slide.

Finally, the TCT plate and the Poly-L-Lysine coated glass slide were under the conditions detailed in table 3.

Once the required time has elapsed (40 min or 48 h), washing steps were carried out in order to extract the L-AA residues that have remained on the surfaces.

The TCT microplate was used to perform fluorescence quenching studies and evaluate the analytical performance of the biosensing platform. On the other hand, Poly-L-Lysine coated glass slides were employed to monitor the reduction process through Raman Spectroscopy.

The changes in GO structure during the reduction process, can be evidenced in the variation of the I_D/I_G ratio, I_D and I_G represent the area under the curve of D and G bands, respectively.

To determine the area under the curve of these bands, the deconvolution process was employed, this process consists of performing a decomposition of the peaks that overlap with each other, thus extracting information from the peaks individually, in this case from the peaks of the D and G bands characteristic of the raman spectrum of graphene oxide. In this way, it is possible to determine the area under the curve of D and G bands individually and obtain the I_D/I_G ratio.

GO and rGO-based Biosensing:

At this stage of experimental set up, photoluminescent probes were made of IgG-FITC. A biorecognition probe composed of the human IgG antibody and the FITC fluorophore was

used. In order to explore GO/rGO adhesion on other surfaces, besides TCT plates, High binding plates were used. Additionally, to carry out fluorescence quenching analyses, the spectrophotometer Cytation 5, BioTek was used.

3.3.1. Kinetic analysis of fluorescence quenching of FITC for different concentrations of GO and bioprobe.

This experiment was designed to find the optimal concentrations of GO and IgG-FITC to maximize fluorescence quenching and it was realized following the configuration presented in Figure 15.

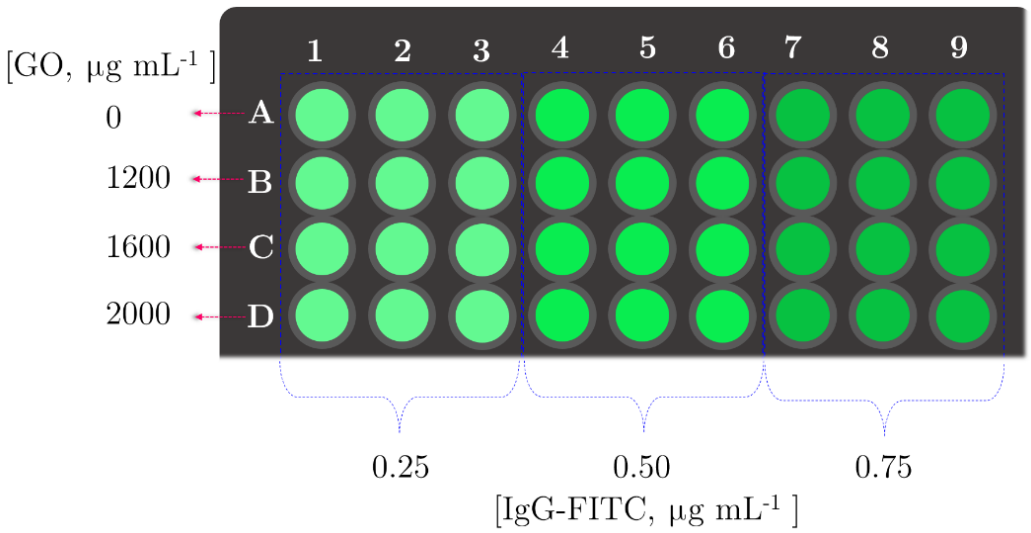

Figure 15 Schematic representation of TCTmicroplate coated with three different concentrations of GO and four different of [IgG-FITC] bioprobe.

TCT plate GO coating and IgG-FITC bioprobe dilution processes were performed similarly to the experiments described in 3.3.1 and using mathematical expression 4.

3.3.2. Kinetics of fluorescence quenching of FITC for a fixed *GO* Concentration and three different IgG-FITC bioprobe concentrations.

According to the results obtained in the previous stage, we employed a GO concentration of 1600 μg mL^{-1} and biorecognition probe concentrations of 0.125, 0.25, 0.5, and 1 μg mL^{-1} as shown in Figure 16.

The bioprobe supplier indicates that the stock concentration of this product is 1 $mgmL^{-1}$, so it was necessary to dilute the IgG-FITC bioprobe employing the serial dilution method. For the dilution process, PBS (phosphate buffered saline) was used, to maintain the physico-chemical conditions of the molecule.

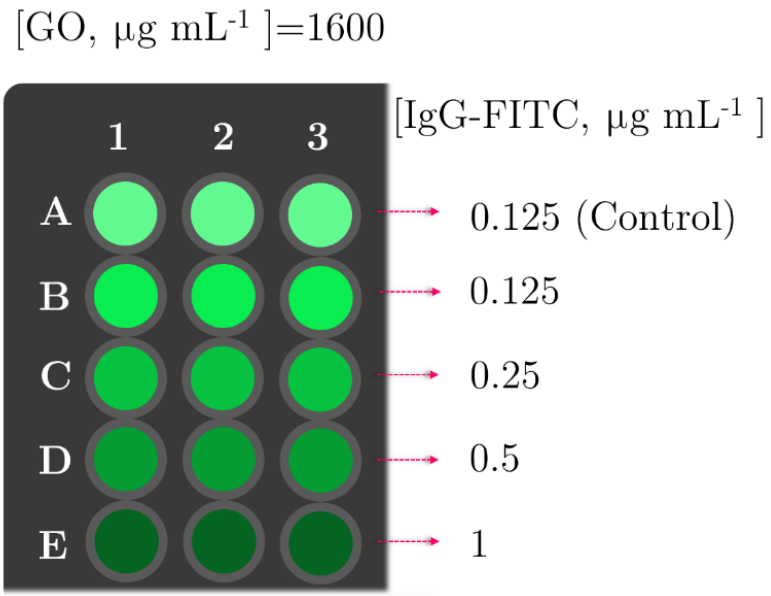

Figure 16 Schematic representation of TCTmicroplate coated with [GO]=1600 μg mL-1 and four different of IgG-FITC bioprobe *concentrations.* After adding the [IgG-FITC] bioprobe (100 μL per well),

the TCT plate was introduced into the spectrophotometer, which had previously been configured according to the parameters summarized in the table 6.

Table 6. Parameters configuration of the spectrophotometer Cytation 5, BioTek

λ excitation (nm)	Parameter to measure	Type of shaking	Shaking frequency	Measurement frequency	Total measurement time
485	Fluorescence emission	Orbital	Every 4 minutes	Every 5 minutes	2 hours

Note: *Orbital shaking can contribute to the homogenization of the solution in the wells.*

3.3.3. Comparison of the kinetics of fluorescence quenching of FITC between CFATA-UNAM samples and GO (commercially available)

As mentioned before, the objective of this work is to achieve an optimization in the sensitivity/assay time of a biosensing system. Therefore, in this stage, studies of kinetic of fluorescence quenching for different GO samples from different synthesis routes are carried out. Here we used samples of GO and rGO synthesized by the Laboratorio de Catálisis CFATA-UNAM research group. The samples have been labelled with numbers 4.1 and 5.1 to indicate that these correspond to two different types of GO.

Another adherence surface and different concentrations of GO and the IgG-FITC bioprobe are also explored. Figure 17 shows the schematic representation for TCT and high binding microplates.

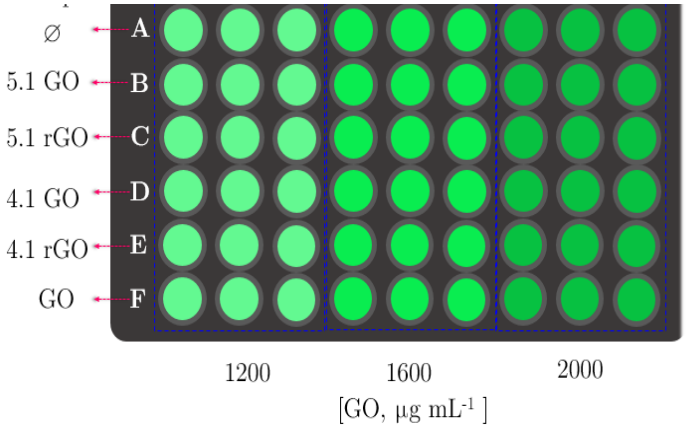

Figure 17 Schematic representation of TCT/High binding microplate coated with different samples and concentrations of GO. One bioprobe concentration is used.

3.3.4. One Phase decay model

To perform a quantitative analysis of quenching kinetics, a nonlinear fit is used. In order to find a theoretical model that fitted the experimental curves correctly, three different nonlinear model were taken into account, however, a model denominated as one phase decay, proved to be the most suitable since it did not present divergences and its χ^2 parameter presented values more closely to 1 than the other adjustments considered.

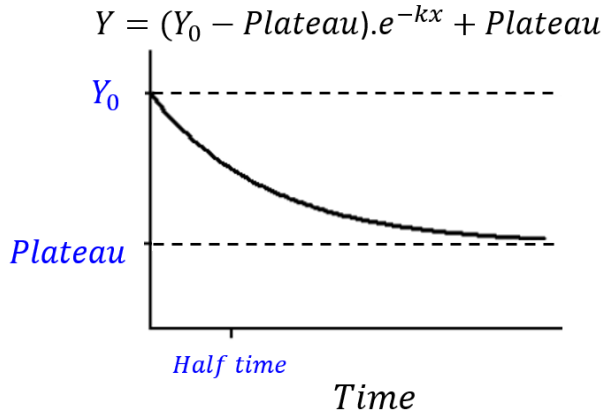

Figure 18 One phase decay model. [63]

3.3.4.1. One phase decay parameters: *Y0 is the Y value when X (time) is zero. It is expressed in the same units as Y,*

- *Plateau is the Y value at infinite times, expressed in the same units as Y.*
- k is the rate constant, expressed in reciprocal of the X axis time units. If X is in minutes, then k is expressed in inverse minutes.
- Tau (x) is the time constant, expressed in the same units as the X axis. It is computed as the reciprocal of K.
- Half-life is in the time units of the X axis. It is computed as $\frac{\ln(2)}{k}$.
- In this case, the most relevant parameters are K, Tau and Plateau values.

Herein, Plateau indicates the levels of fluorescence quenching, the k represents fluorescence quenching saturation speed and Tau is the time when fluorescence quenching saturation takes place.

REFERENCES

(60) Corning 2014, Cell culture surfaces CLS-C-DL-006_REV2_DL.Pdf.

(61) Corning and Falcon Microplates Selection Guide, Cell culture surfaces, CLS-C-DL-MP-014REV9.Pdf.

(62) Zhang, J.; Yang, H.; Shen, G.; Cheng, P.; Zhang, J.; Guo, S. Reduction of Graphene Oxide ViaL-Ascorbic Acid. Chem. Commun. 2010, 46 (7), 1112–1114. https://doi.org/10.1039/B917705A

CHAPTER 4.

RESULTS AND DISCUSSION

In this chapter the results of the experiments developed in the experimental methods chapter are reported. These results display some changes in the analytical performance of the biosensing platform related to the reduction of GO, such changes and results will be discussed below.

4.1.GO adhesion on TCT microplate surface

The microplates employed for this study were the TCT (tissue culture treated) type. The polystyrene surface of this microplates has been previously modified by amino groups, positively charged that favor the adhesion of cells to the surface. [60] On the other hand, the GO in aqueous suspension presents a negative charge, [64] so its adhesion onto TCT microplate surface is given, mainly by electrostatic interactions.

Results of adhesion studies obtained through Raman spectra analysis (Figure 18 and 19), indicates a relationship between Raman intensity and GO concentration. Raman intensity increases when GO concentration also does, however, in Figure 21 we can observe that the

values corresponding to the concentration of 1400 do not follow the same behavior as the concentrations 1200 and 1600 μg mL^{-1} with respect to the Raman intensity.

The explanation for this inconsistency, is related to the fact that some of the parameters that had to remain fixed were altered by mistake during the spectrum acquisition. Specifically, the size of the laser spot used to focus the samples with concentrations 1600 and 2000 μg mL^{-1} was different from that for the sample with concentration 1400 μg mL^{-1}.

For this reason, the GO adhered values for 1400 μg mL^{-1} concentration were not taken into account.

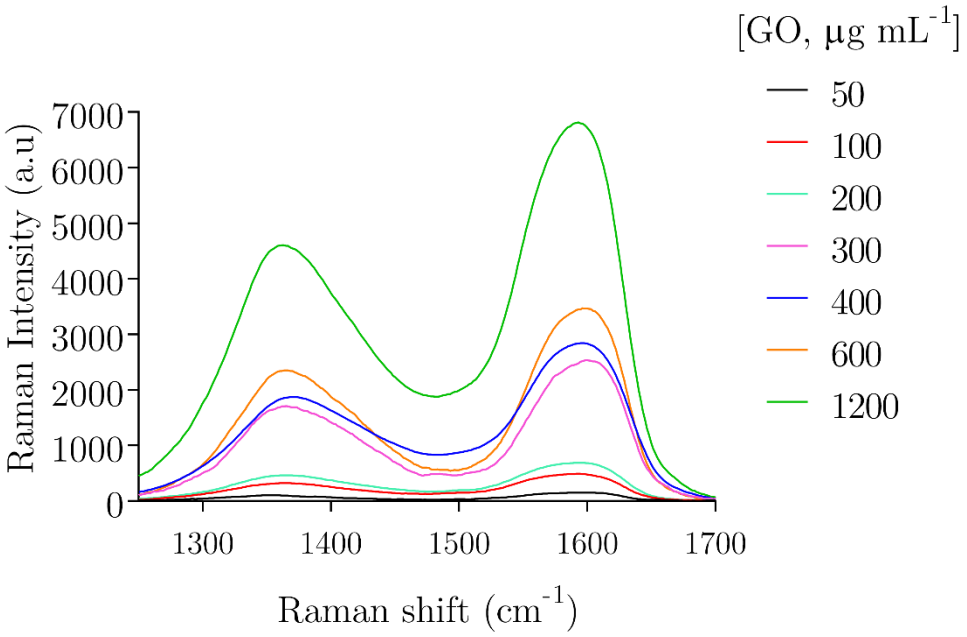

Figure 19 Raman spectra of different drop-coated GO concentrations (without washes stages)

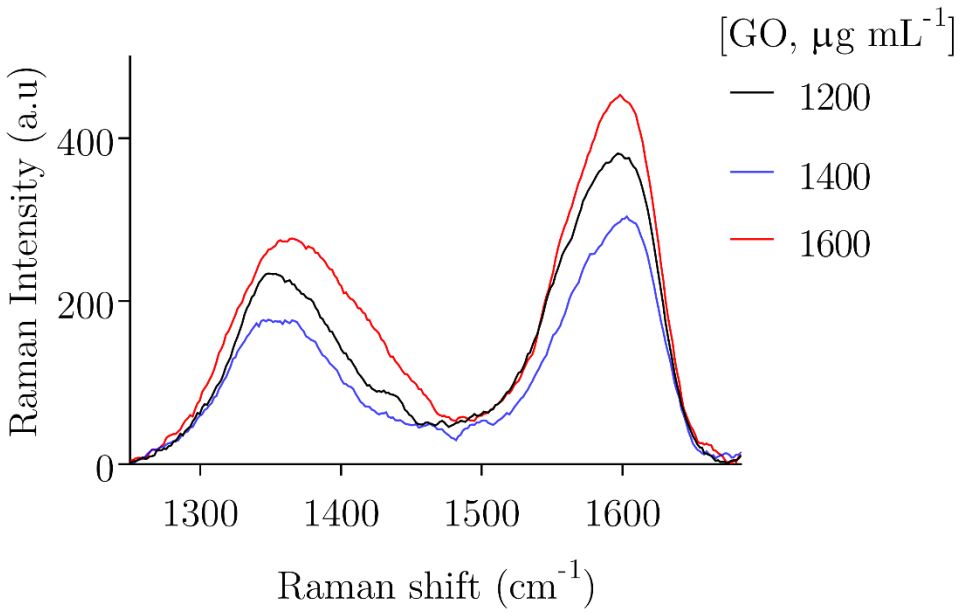

Figure 20 Raman spectra of the incubated samples after several washes.

The explanation for this inconsistency, is related to the fact that some of the parameters that had to remain fixed were altered by mistake during the spectrum acquisition. Specifically, the size of the laser spot used to focus the samples with concentrations 1600 and 2000 μg mL^{-1} was different from that for the sample with concentration 1400 μg mL^{-1}.

Additionally, we made a linear interpolation (Figures 21 and 22), this adjustment provided information about the amount of graphene adhered after the washing stages.

The peak values of the D and G bands in Figure 16 were replaced in the y variable of the corresponding linear settings. The estimated GO concentration value is obtained solving the linear equation for x.

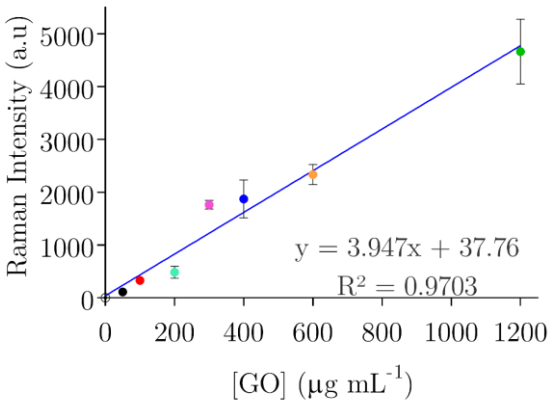

Figure 21 Calibration curve with G peak intensities.

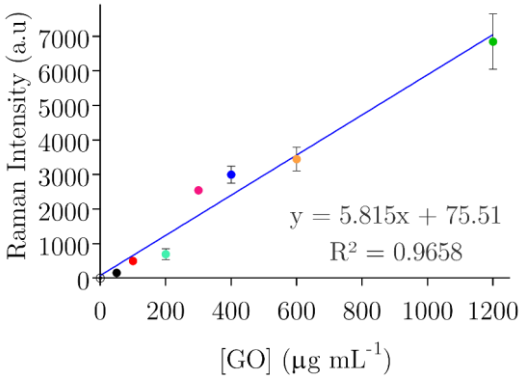

Figure 22 Calibration curve with G peak intensities.

Table 7 and 8 show the estimated values obtained from the calibration curves for the D and G peaks respectively.

Table 7. Estimation of GO adhered (D peaks intensity).

[GO] (µg mL^{-1})	**[GO Adhered] (µg mL^{-1})**	**GO Adhered (%)**
1600	71.473 ± 17.50	4.47
1400	44.128 ± 6.78	3.15
1200	67.626 ±9.59	5.63

Table 8. Estimation of GO adhered (G peaks intensity).

[GO] (µg mL^{-1})	**[GO Adhered] (µg mL^{-1})**	**GO Adhered (%)**
1600	71.674 ± 15.60	4.48
1400	45.38 ± 9.202	3.24
1200	61.45 ± 16.764	5.12

According to tables 7 and 8, around 5% of the incubated GO is attached onto the wells.

This is information is relevant in order to proceed with the proposed reduction process efficiently.

4.2.Characterization of reduction process.

Two routes were considered for the reduction process, the first one consisted in subjecting the rGO coated microplate to a temperature of 90 °C for 40 minutes. The second route was to leave the sample at room temperature for 48 hours (Table 2).

In the first case, no results were obtained, since, when performing the Raman spectroscopy study, no graphene signal was presented. It is possible that this was such an aggressive method that the GO adhered to the surface was removed in the reduction process.

On the other hand, for the second reduction route, Raman signal were obtained for reductions 1.75 and 3.5 × [GO] the samples (see Figures 25 and 26).

Table 9 summarizes the results of the deconvolution of the GO Raman spectrum before the reduction process, so that, the I_D/I_G ratio is taken as a point of comparison between the I_D/I_G values of Tables 10 and 11.

Table 9. I_D/I_G ratios for GO (commercially available)

[GO] (μg.mL^{-1})	
I_D/I_G	χ^2
0.96	0.996

Taken as a reference, the I_D / I_G relationship of table 9, it is possible to see in table 10

and 11, that the reduced GO presents a decrease in this value, this allows us to show that the reduction process is being effective.

Now, comparing the results between Tables 10 and 11, it is possible to determine that the reduced GO by 3.5 × [GO] presents a greater consistency or regularity in the I_D/I_G values than 1.75 × [GO]. This leads us to explore other reduction processes around 3.5 ×[GO].

Table 10 I_D/I_G ratios for GO reduced by 1.75×[GO]

[rGO 1.75×] (μg mL^{-1})	**I_D/I_G**	**χ^2**
60	0.730	0.983
80	0.860	0.989
100	0.895	0.959

Table 11 I_D/I_G ratios for GO reduce by 3.5×[GO]

[rGO 3.5×] (μg mL-1)	**I_D/I_G**	**χ^2**
60	0.790	0.995
80	0.802	0.994
100	0.817	0.993

Raman spectrum of each of the reduction processes are presented as well as the respective fitting are shown in appendix, Figures A-1 and A-2, respectively.

4.2.1. Kinetic fluorescence quenching at [GO]=1600 μg mL^{-1}

Kinetics fluorescence quenching study is a very useful tool because it allows to determine to what extent the fluorescence of a fluorophore, in this case FITC, is affected over time due to the interaction with the GO. In other words, the kinetic quenching study can also indicate about the fluorescence quenching capability of GO.

The study of the kinetics fluorescence quenching at a fixed concentration of GO and four different concentrations of bioprobe (see Figure 23), confirms that [IgG-FITC] = 0.5 μg mL^{-1} is the most efficient fluorescence quenching when the microplate is covered with [GO] = 1600 μg $mL^{-1.}$

The analytical performance of this biosensing platform is our starting point, therefore, the plateau parameter value (0.3248) and Tau parameter value (31.85) shown in Table 2 must be taken into account in order to compare and identify the effects caused after the reduction of GO.

NOTE: It is important to clarify that photoluminescence quenching phenomenon was measured by dividing the final photoluminescence intensity I_f (at 120 min) by the initial photoluminescence intensity (I_0 at 0 min). Hence, I_f/I_0 values around 1 show a weak photoluminescence quenching phenomenon, whereas I_f/I_0 values around 0 prove a strong photoluminescence quenching phenomenon.

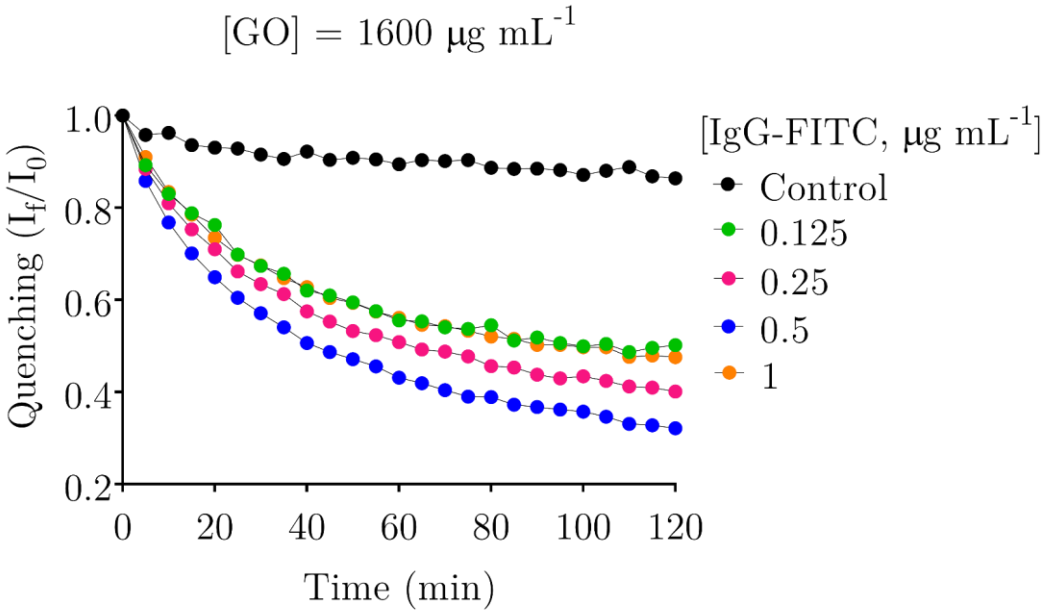

Figure 23 Kinetics of fluorescence quenching for FITC. Control ([IgG-FITC] = 0.125 µg mL⁻¹).

Table 12. Fitting parameters for GO (before reduction process)

[GO]= 1600 µg.mL⁻¹

[IgG-FITC]= µg.mL⁻¹	Control	0.125	0.25	0.5	1
Plateau	0.8725	0.4849	0.3982	0.3248	0.4698
K(au.min⁻¹)	0.0257	0.0314	0.02915	0.0314	0.0300
Tau (min)	38.9105	31.8471	34.305	31.8471	33.33
χ^2	0.7108	0.9717	0.8841	0.9424	0.9552

4.2.2. Kinetics with GO(commercial) after reduction process

After performing and characterizing the reduction process of commercial GO (Section 4.2), the kinetics fluorescence quenching experiments were made this in order to evidence the fluorescence quenching ability of the reduced GO (rGO). Here we use two IgG-FITC concentrations, 0.17 and 0.5 μg mL^{-1}.

Figures 24 and 25 display the kinetics of fluorescence quenching of the biosensing platforms coated with rGO generated by the 1.75 × [GO] and 3.5 × [GO] reduction processes respectively.

According to the adjustment parameters related to the quenching ability shown in these tables, there is no evidence of improvement with respect to the biosensor platform corresponding to Figure 23. However, it is observed that the fluorescence quenching saturation time is shorter than in the case of Figure 22, this value ranges from 31.847 min to 25.68 and 25.94 min.

Tables 13 and 14 contrast the reduction levels, leaving the concentration of the IgG-FITC bioprobe as a constant parameter.

In table 13, no notable differences are observed between the effects generated by the rGO reduced by 1.75 × [GO]and the one reduced by 3.5× [GO] this may also be due to the fact that the concentration of the bioprobe is not the most adequate for the concentrations of

rGO present in the surface. It is necessary to explore more reduction processes with new amounts of L-AA and concentration of IgG-FITC.

Table 14 indicates that there was no improvement in the analytical performance parameters, since for this case, the fluorescence quenching levels are on average of and the saturation times exceed 30 min (**rGO 3.5×[GO] case**). Similar to the case shown in Table 13, more tests should be performed with different concentrations of the bioprobe to optimize the interaction between the bioprobe and the rGO.

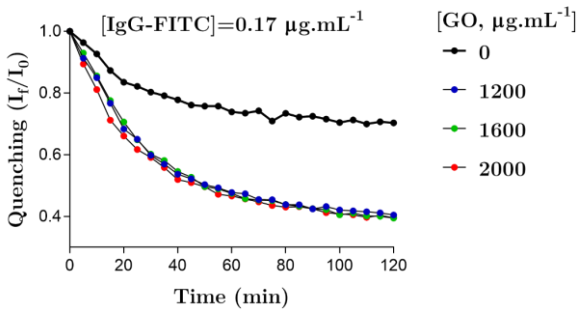

Figure 24 Kinetics of fluorescence quenching for 1.75×[GO] reduction.

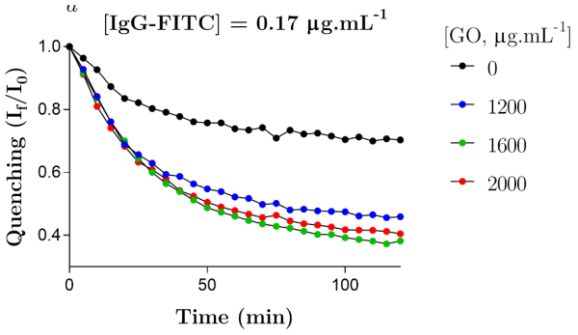

Figure 25 Kinetics of fluorescence quenching for 1.75×[GO] reduction.

Table 13. Comparison: Equal concentration of IgG-FITC and different reduction degree.

[GO] (µg.mL^{-1})	[IgG-FITC]= 0.17 µg.mL^{-1}					
	rGO 1.75×[GO]			rGO 3.5×[GO]		
	Plateau	*k* (au.min^{-1})	Tau (min)	Plateau	*k* (au.min^{-1})	Tau (min)
1200	0.406	0.0364	27.51	0.4609	0.03855	25.94
1600	0.3917	0.0341	29.36	0.3695	0.03299	30.31
2000	0.4010	0.0389	25.68	0.409	0.03668	27.26

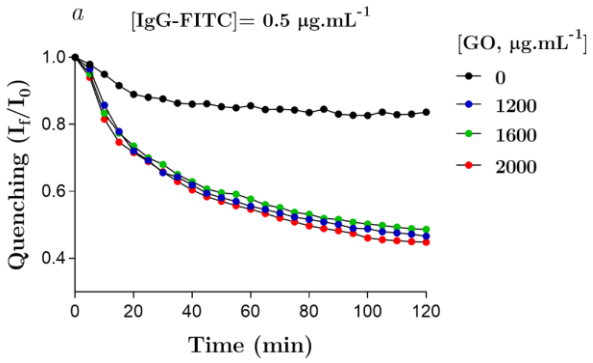

Figure 26 Kinetics of fluorescence quenching for 1.75×[GO] reduction.

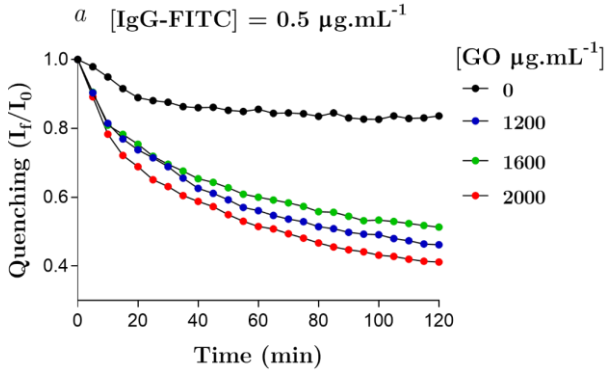

Figure 27 Kinetics of fluorescence quenching for 1.75×[GO] reduction.

Table 14. Comparison: Equal concentration of IgG-FITC and different reduction degree.

[GO] (µg.mL^{-1})	[IgG-FITC]= 0.5 µg.mL^{-1}					
	rGO 1.75×[GO]			rGO 3.5×[GO]		
	Plateau	k (au.min^{-1})	Tau (min)	Plateau	k (au.min^{-1})	Tau (min)
1200	0.4712	0.0333	30.04	0.4553	0.02757	36.28
1600	0.4877	0.0325	30.80	0.5152	0.03002	33.31
2000	0.4472	0.0313	31.99	0.4141	0.0305	32.78

Tables 15 and 16 present a comparison between the samples that were reduced under the same reduction proportion (1.75 × [GO] or 3.5 × [GO]), and interact with different concentrations of IgG-FITC in photoluminescent quenching.

From Table 17 it can be seen that, besides to the degrees of reduction, the relationship between GO and IgG-FITC concentrations plays an important role in the analytical performance of this biosensing platform. GO samples interacting with a concentration of [IgG-FITC] = 0.17 exhibited better quenching values and shorter fluorescence quenching

saturation time than those interacting with [IgG-FITC = 0.5].

Table 15. Comparison: Equal reduction degree and different concentration of IgG-FITC.

rGO 1.75×[GO]

[GO] (μg.mL^{-1})	[IgG-FITC μg.mL^{-1}]					
	0.17			0.5		
	Plateau	k (au.min^{-1})	Tau (min)	Plateau	k (au.min^{-1})	Tau (min)
1200	0.406	0.0364	27.51	0.4712	0.0333	30.04
1600	0.3917	0.0341	29.36	0.4877	0.0325	30.80
2000	0.4010	0.0389	25.68	0.4472	0.0313	31.99

Table 16. Comparison: Equal reduction degree and different concentration of IgG-FITC.

rGO 3.5×[GO]

[GO] (μg.mL^{-1})	[IgG-FITC μg.mL^{-1}]					
	0.17			0.5		
	Plateau	k (au.min^{-1})	Tau (min)	Plateau	k (au.min^{-1})	Tau (min)
1200	0.4609	0.03855	25.94	0.4553	0.02757	36.28
1600	0.3695	0.03299	30.31	0.5152	0.03002	33.31
2000	0.409	0.03668	27.26	0.4141	0.0305	32.78

4.3.Samples provided by Laboratorio de Catálisis CFATA-UNAM research group

The quenching abilities of the samples 4.1, 5.1 GO and rGO provided by Laboratorio de Catálisis CFATA-UNAM group were explored and compared with the commercial GO.

- **Onto TCT microplate surface**

In figure 28 it can be seen that 4.1 rGO has better abilities as a fluorescence quencher than 4.1GO, which agrees with the hypothesis established for this work.

Table 17 shows the fitting parameters for samples 4.1GO and 4.1rGO when the microplate with the TCT surface was employed. From this table, it can be seen that for [GO] = 1200 μgmL^{-1} and improvement in quenching abilities is more evident with respect to the non-reduced sample from 0.73 to 0.72. Regarding the saturation time of photoluminescence quenching, it goes from 33.05 minutes to 27.6 min after reduction.

Table 18, no notable change was observed between these samples due to reduction process.

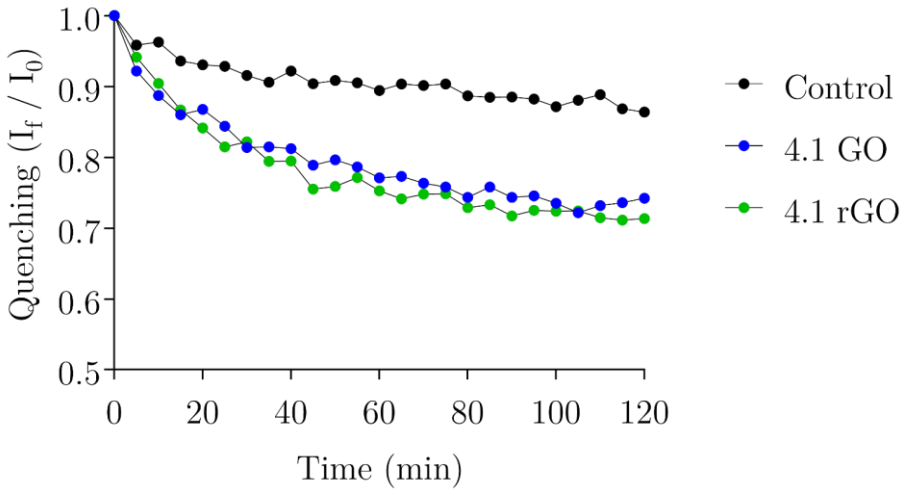

Figure 28 Kinetics of fluorescence quenching using samples of 4.1 GO and 4.1 rGOon TCT microplate surface

Table 17. Comparison: Equal concentration of IgG-FITC and different reduction degree of 4.1 samples onto TCT microplate surface.

[GO] (µg.mL^{-1})	[IgG-FITC]= 0.125 µg.mL^{-1}					
	4.1GO			4.1 rGO		
	Plateau	*k* (au.min^{-1})	Tau (min)	Plateau	*k* (au.min^{-1})	Tau (min)
1200	0.7297	0.03026	33.05	0.717	0.03622	27.61
1600	0.7348	0.03552	28.15	0.7368	0.03792	26.37
2000	0.7565	0.03826	26.14	0.736	0.03104	32.21

In this case, figure 24 indicates that the 5.1rGO sample did not exhibit an improvement in quenching ability of 5.1GO according to the hypothesis.

Regarding the fitting parameters of the 5.1 GO and 5.1rGO samples, showed in Table 18, no notable change was observed between these samples due to reduction process.

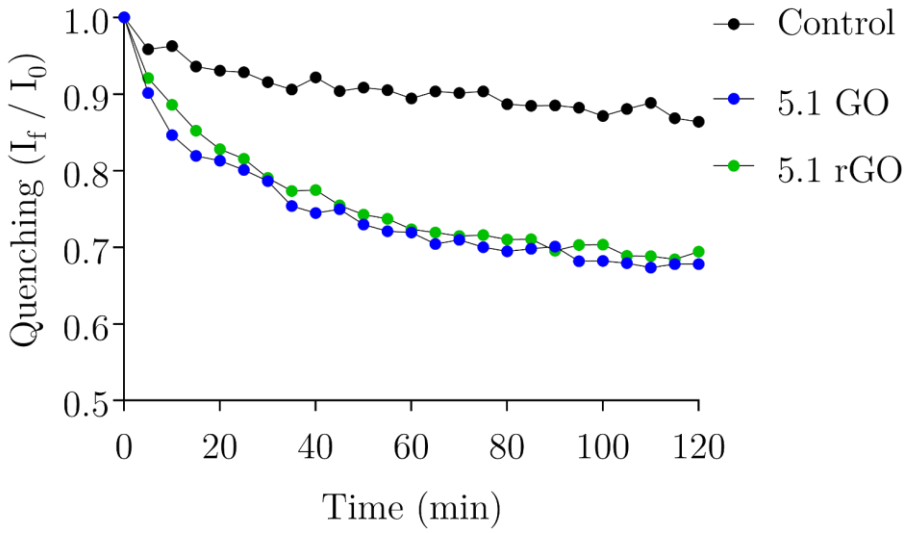

Figure 29 Kinetics of fluorescence quenching using samples of 5.1 GO and 5.1 rGO on TCT microplate surface.

Table 18. Comparison: Equal concentration of IgG-FITC and different reduction degree of 5.1 samples onto TCT microplate surface.

[GO] (μg.mL^{-1})	[IgG-FITC]= 0.125 μg.mL^{-1}					
	5.1GO			5.1 rGO		
	Plateau	*k* (au.min^{-1})	Tau (min)	Plateau	*k* (au.min^{-1})	Tau (min)
1200	0.68	0.03734	26.78	0.6887	0.03464	28.87
1600	0.653	0.04182	23.91	0.6952	0.03132	31.93
2000	0.7118	0.04904	20.39	0.7075	0.03815	26.21

- **Onto high binding surface**

Now, in the case that the surface covered was high binding type, the fitting parameters presented in Tables 19 and 20, besides to indicate improvements in the quenching abilities, have fluorescence saturation times between 10-12, These times are the smallest of the experiments performed until now.

It is important not to overlook that in Figures 30 and 31, the fluorescence quenching presents a rapid saturation compared to previous experiments, this is reflected in the Tau. parameter of the table 19 and 20.

The improvement in saturation times is directly related to the interaction or affinity between this surface and the GO and rGO samples.

According to the information presented by the manufacturer, the high binding surface is designed for hydrophobic and ionic interactions. This surface is negatively charged, which is a bit contradictory, because GO in aqueous solution has a negative net charge and should

not be related, at least electrostatically, so it is possible to attribute this affinity to other characteristics such as lateral size or the degree of reduction of these samples.

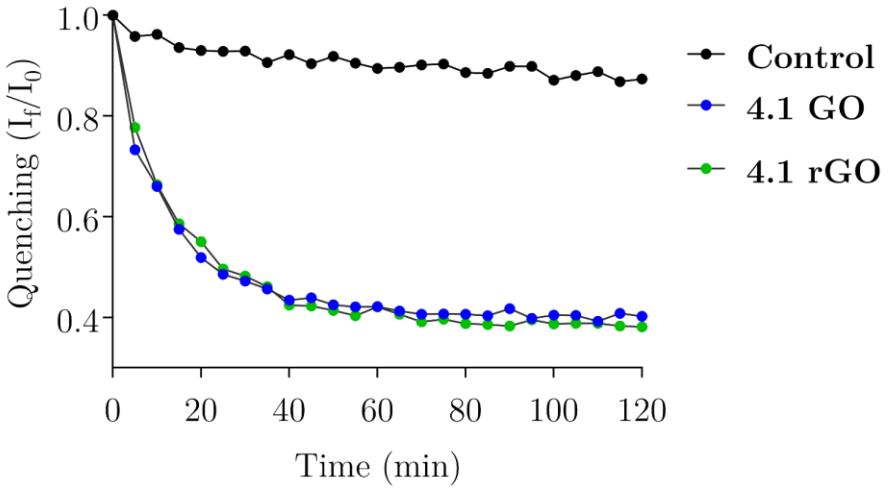

Figure 30 Kinetics of fluorescence quenching using samplesof 4.1 GO and 4.1rGOon High binding microplate surface

Table 19. Comparison: Equal concentration of IgG-FITC and different reduction degree of 4.1samples onto High binding microplate surface.

[GO] (µg.mL^{-1})	[IgG-FITC]= 0.125 µg.mL^{-1}					
	4.1GO			4.1 rGO		
	Plateau	*k* (au.min^{-1})	Tau (min)	Plateau	*k* (au.min^{-1})	Tau (min)
1200	0.4094	0.08305	12.04	0.3914	0.06985	14.32
1600	0.3917	0.09066	11.03	0.4477	0.09477	10.55
2000	0.4176	0.08267	12.10	0.4445	0.08004	12.49

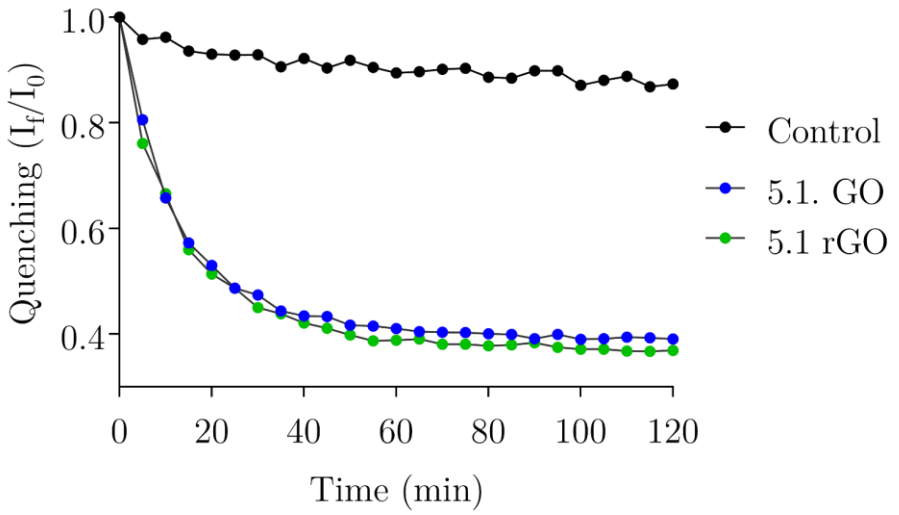

Figure 31 Kinetics of fluorescence quenching using samples of 5.1 GO and 5.1rGOon High binding microplate surface

Table 20. Comparison: Equal concentration of IgG-FITC and different reduction degree of 5.1samples onto High binding microplate surface.

[GO] (µg.mL^{-1})	**[IgG-FITC]= 0.125 µg.mL^{-1}**					
	5.1GO			**5.1 rGO**		
	Plateau	k **(au.min^{-1})**	**Tau (min)**	**Plateau**	k **(au.min^{-1})**	**Tau (min)**
1200	0.399	0.07705	12.98	0.3779	0.07426	13.47
1600	0.3475	0.08328	12.01	0.422	0.08976	11.14
2000	0.3933	0.08289	12.06	0.3938	0.07665	13.05

REFERENCES

(63) Lerf, A. Graphite Oxide Story – From the Beginning Till the Graphene Hype. In *Graphene Oxide*; John Wiley & Sons, Ltd, 2016; pp 1–35. https://doi.org/10.1002/9781119069447.ch1.

(64) GraphPad Prism 7 Curve Fitting Guide - Equation: One phase decay https://www.graphpad.com/guides/prism/7/curve-fitting/reg_exponential_decay_1phase.htm (accessed Aug 1, 2020).

CHAPTER 5.

CONCLUSIONS

- In the present work, the effects generated in the analytical performance of a biosensing platform due to the reduction of GO (commercially available) and samples of GO and rGO provided by the Laboratorio de Catálisis CFATA-UNAM research group were analyzed and evidenced.

- The results in this work are relevant because from them, an experimental route can be outlined in order to explore new parameters and thus to achieve an optimization in the analytical performance of the biosensing platform.

- Besides to the levels of GO reduction, the affinity between surfaces (TCT and High binding) and GO as well as concentrations of GO / IgG-FITC were also taken into account, since these have an effect on photoluminescence quenching of FITC and the analytical performance in general.

- The best experiment of photoluminescence quenching performed with the GO (commercially available) onto TCT microplate surface, indicated that its quenching ability corresponded to a value of 0.32 and a photoluminescence quenching saturation time of 32 min, after the reduction process the quenching value was 0.40

and the photoluminescence quenching saturation time was reduced to 25.68 min. This decrement is directly related with the improvement in the analytical performance associated to the assay time since it will allow to obtain faster results.

- On the other hand, the samples provided by the CFATA-UNAM research group displayed lower affinity to the TCT surface, a fact that was reflected in a decrease in the fluorescence quenching ability, when the TCT surface was replaced by the High binding surface, the fluorescence quenching values changed from 0.74 to 0.4 and 0.71 to 0.38 form 4.1GO and 4.1rGO samples respectively. In 5.1 case the fluorescence quenching values were from 0.68 to 0.39 and 0.69 to 0.37 for 5.1 GO and rGO, respectively. Conversely, GO (commercially available) presented a higher affinity for the TCT surface displaying better fluorescence quenching ability. In TCT the quenching value were 0.32, while on the High binding surface the value was 0.43. Here we have an evidence that exist structural differences between GO (commercially available) sample and those synthesized by the Laboratorio de Catálisis CFATA-UNAM research group.

- Additionally, on TCT and High binding microplate surface the reduced 4.1GO has advantages over the 4.1GO regarding the quenching ability and photoluminescence saturation time as established by the hypothesis. While the sample 4.1 rGO presents in its best experiment a value of 0.71 units of quenching, the sample of 4.1 GO, also in its best experiment presents values of 0.74. In addition, regarding the fluorescence saturation time, 4.1 GO offers photoluminescence saturation times of 33 minutes

while 4.1 rGO of 27 min.

- In the case of 5.1GO and 5.1 rGO samples, they did not exhibit the behavior according to the hypothesis, however the fluorescence quenching values show that 5.1GO/rGO samples are more efficient than 4.1GO/rGO samples, since the quenching values on TCT/High binding microplate surface were 0.68/0.39 and 0.69/0.37 for 5.1 GO and 5.1 rGO correspondingly, for 4.1 GO and 4.1 rGO the quenching values were 0.74/0.40 and 0.71/0.38 respectively.

- Respect with assay time, 5.1 GO/rGO exhibited, more efficiency in photoluminescence quenching saturation time than 4.1GO/rGO. In the best experiment performed to 5.1GO and 5.1 rGO on TCT/High binding microplate surface the times obtained were 23/12 and 28/11 minutes, for 4.1GO an4.1rGO the times were 33/11 and 27/10.55 minutes.

- Finally, in order to compare how effective our reduction process was with respect to samples 4.1 and 5.1 rGO, it was observed that in the best experiments in which microplates with high binding surface were used, the levels of quenching for these samples were 0.39 and 0.35 (4.1 and 5.1 rGO respectively), while for the rGO (commercially available) on TCT microplate surface the quenching values were 0.36. Additionally, for each of the fluorescence values presented above, the corresponding times were 11 and 12 minutes while for the rGO (commercially available), the time was 30 min. In other words, although the rGO has abilities as a photoluminescence

quencher, it does not reach the saturation of the photoluminescence quenching as quickly as was evidenced in the reduced samples of Laboratorio de Catálisis CFATA-UNAM research group.

- The lateral size of GO flakes and the C/O ratio, these values would be of great relevance to deeply understand the obtained results and thus optimize the properties of these samples.

OUTLOOK

With the aim of achieving a complete study on the effects that the reduction of GO generates in a biosensing platform, we intend to continue with the experimental route that had been constructed once the contingency period ends.

Nowadays, biosensors are widely used tools in various fields as a medic, food analysis and environmental monitoring, etc., it is highly relevant to have devices that offer reliable results, low cost and with a short response time for rapid result. We consider that the experimental evidence of this project, such as enhancement in fluorescence quenching or the decrease in photoluminescence saturation time due to the reduction process on GO samples, can be relevant to optimize the sensitivity and assay time of GO / rGO-based biosensors.

CHAPTER 6. APPENDIX

6.1.Raman Spectrum of reduced GO

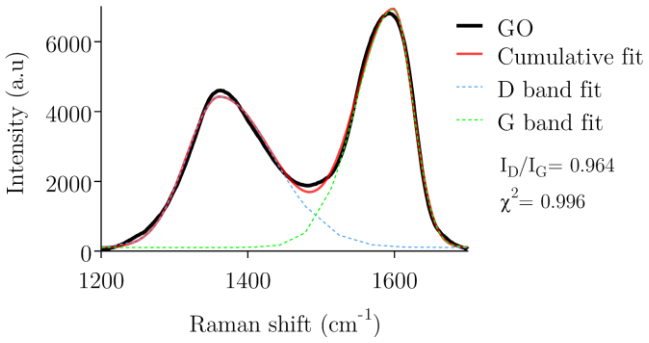

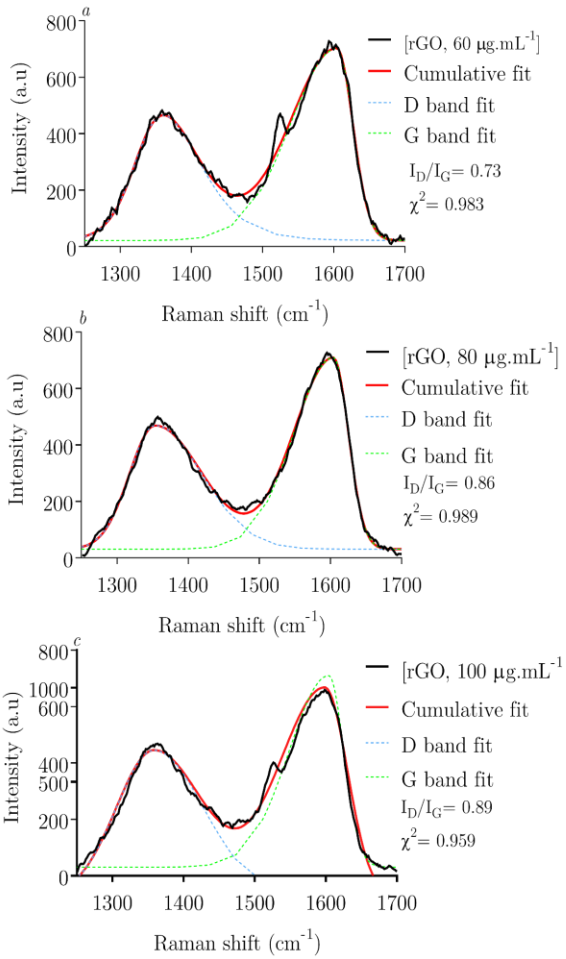

Figure A- 1: Raman spectrum of 1.75×[GO] reduction process with D, and G band fitting

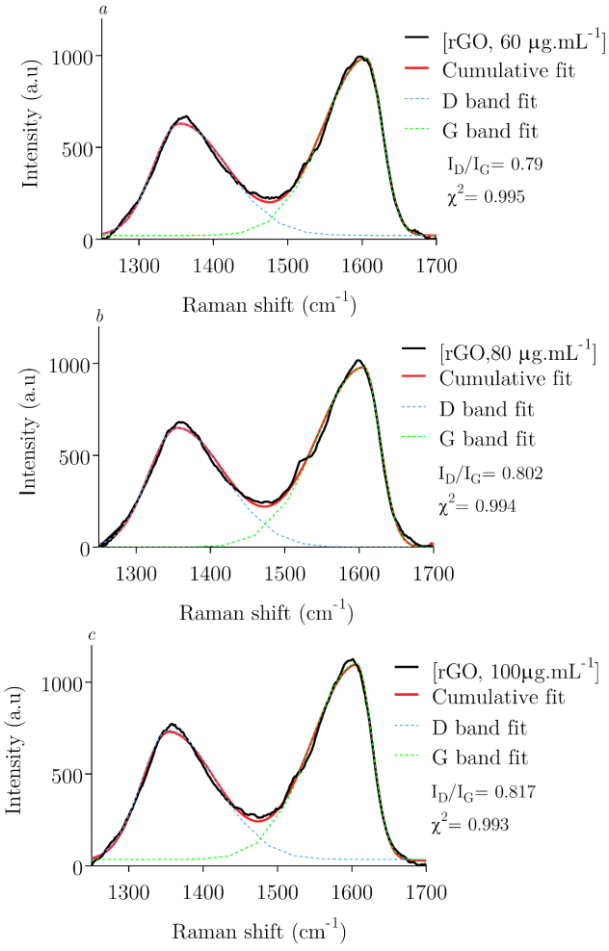

Figure A- 2 Raman spectrum of 1.75×[GO] reduction process with D, and G band fitting

6.2.Kinetic fluorescence quenching for different [GO] and [IgG-FITC].

Figures A-4 to A-6 show the behavior of fluorescence quenching for different [GO] and [IgG-FITC]. From this, it is possible to evidence that the highest quenching of fluorescence occurs for [GO] = 1600 μg mL^{-1} and [IgG-FITC] = 0.5 μg mL^{-1} case (from Figure 28), however the biorecognition probe presents better stability for a concentration of 0.75 μg mL^{-1}.

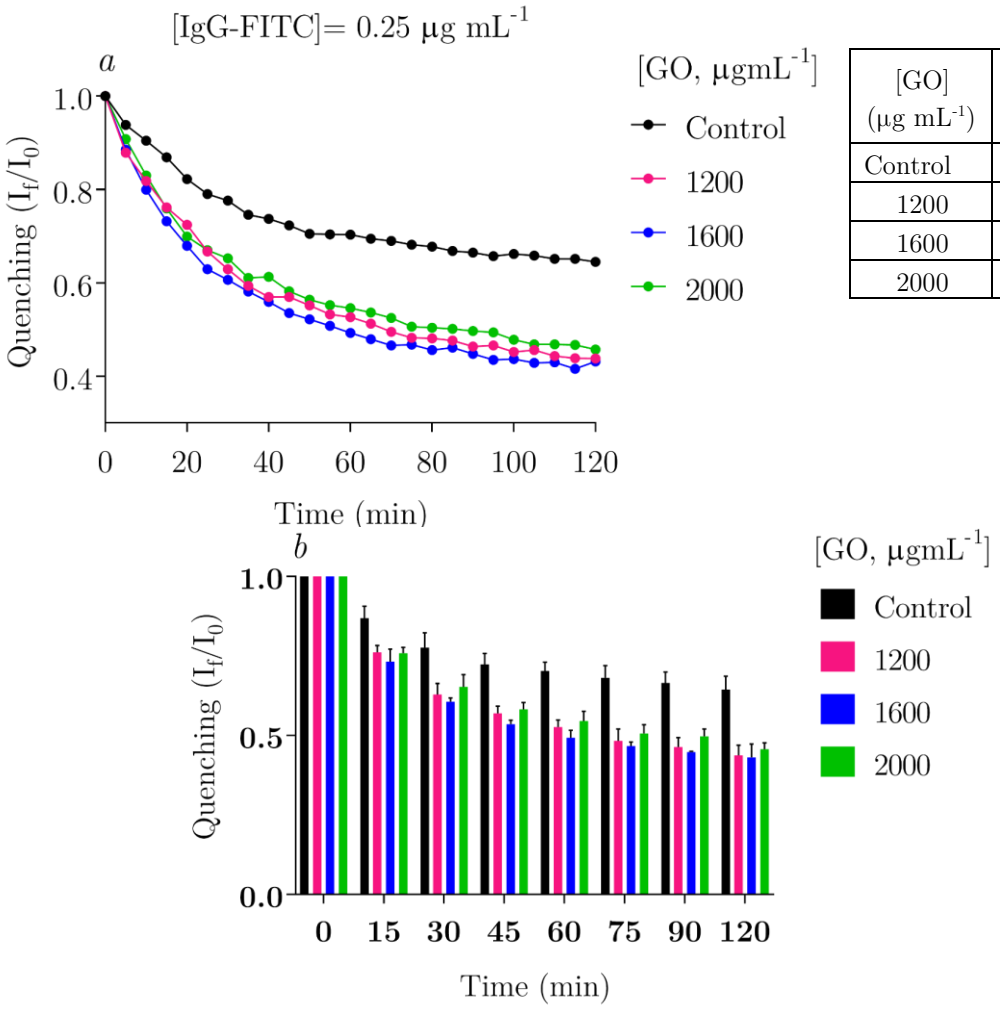

[GO] (μg mL^{-1})	I_f/I_0
Control	0.65
1200	0.43
1600	0.43
2000	0.46

Figure A- 3 Kinetic fluorescence quenching
a. Kinetics of fluorescence quenching for different[GO] and [IgG-FITC] = 0.25 μg mL-1. b. Kinetic

fluorescence quenching bar graphs.

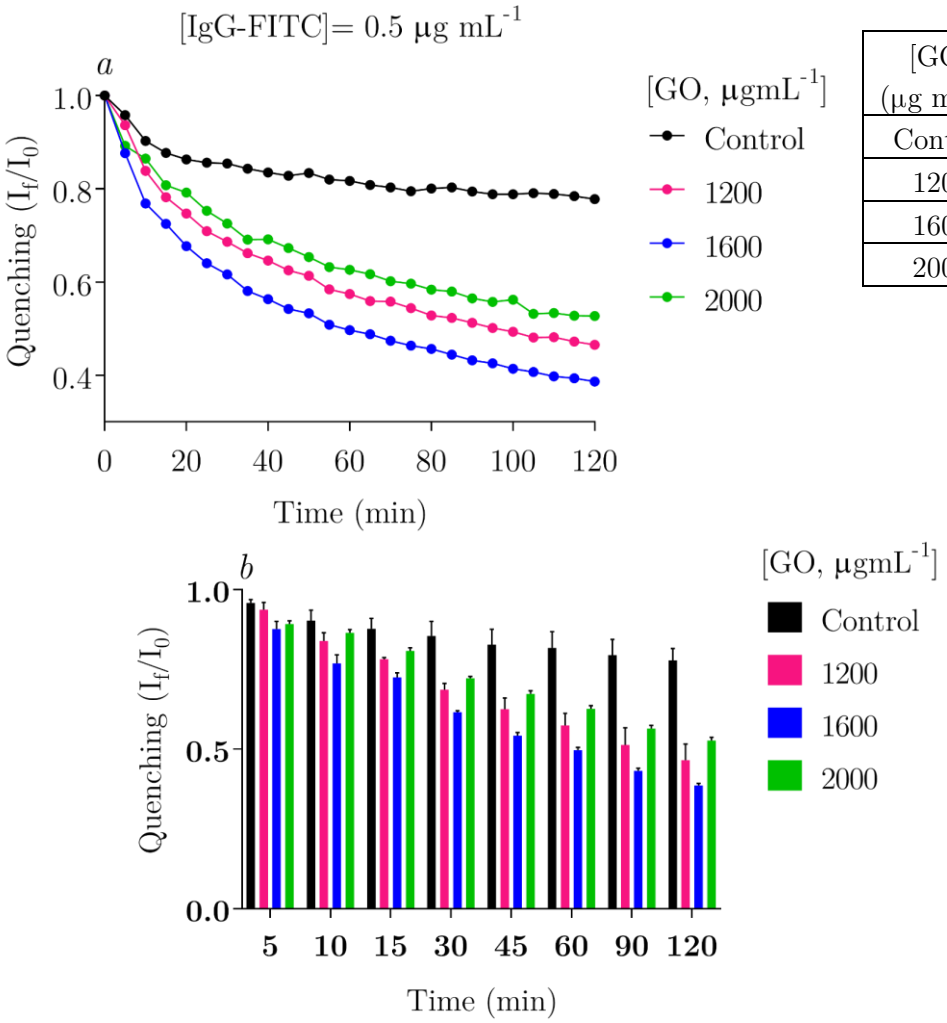

[GO] (µg mL^{-1})	I_f/I_0
Control	0.77
1200	0.46
1600	0.39
2000	0.53

Figure A- 4Kinetics of fluorescence quenching a. Kinetics of fluorescence quenching for different[GO] and [IgG-FITC] = 0.5 µg mL-1. b. Kinetic fluorescence quenching bar graphs

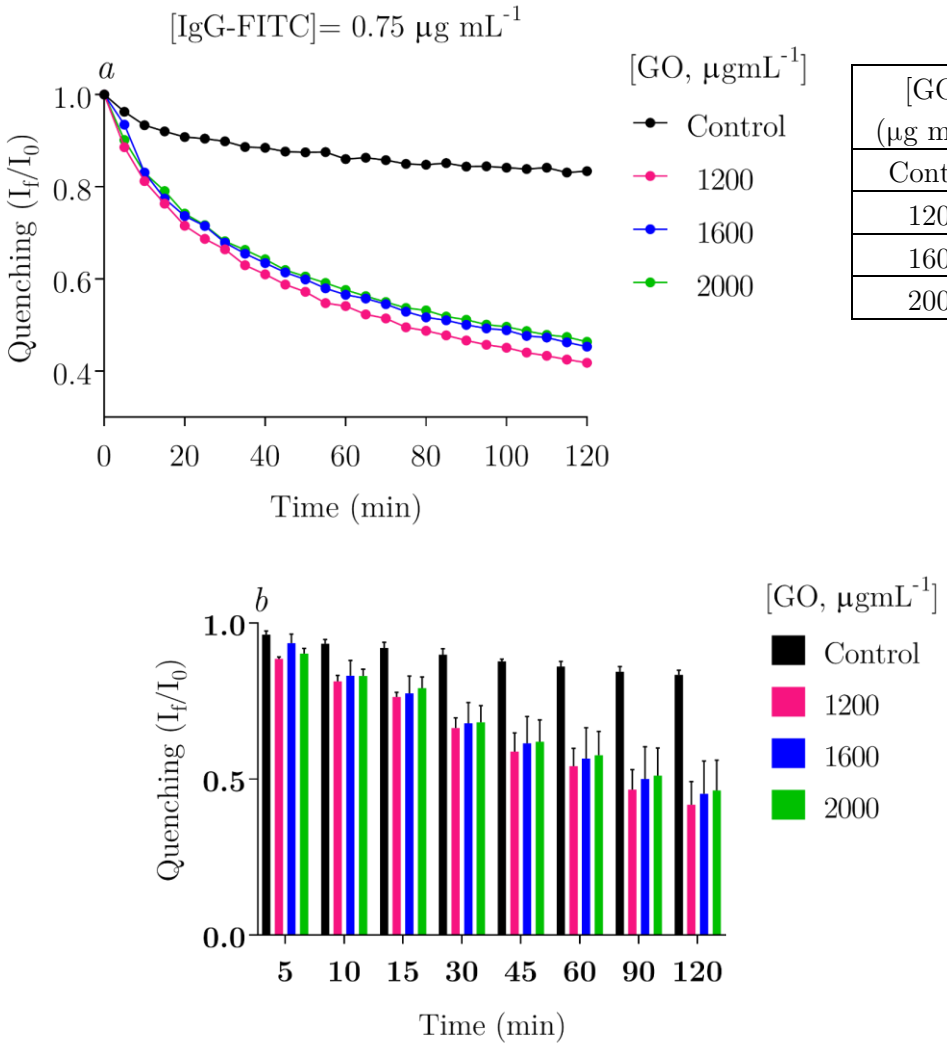

[GO] (µg mL^{-1})	I_f/I_0
Control	0.83
1200	0.41
1600	0.45
2000	0.46

Figure A- 5Kinetics of fluorescence quenching a. Kinetics of fluorescence quenching for different[GO] and [IgG-FITC] = 0.75 µg mL-1. b. Fluorescence quenching bar graphs.

6.3.Kinetic fluorescence quenching at [GO]=1600 μg mL^{-1} (bar graphs)

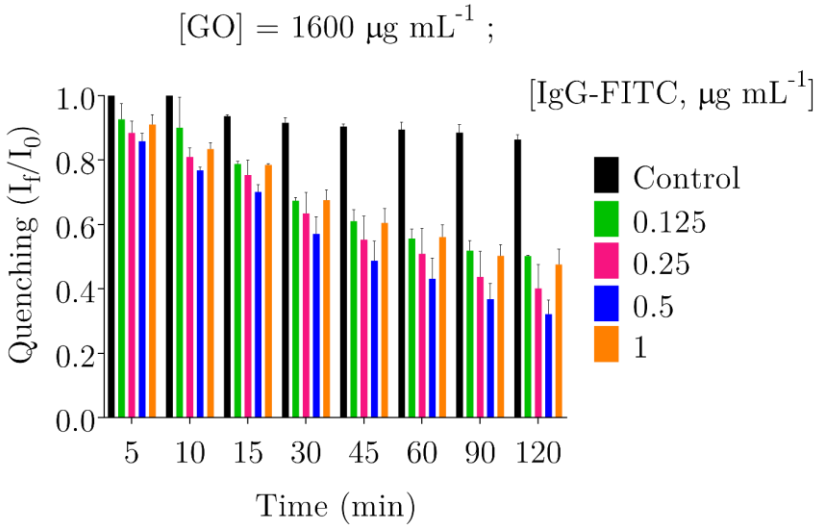

Figure A- 6 Kinetics of fluorescence quenching bar graphs.

6.4.Kinetic fluorescence quenching (bar graphs)

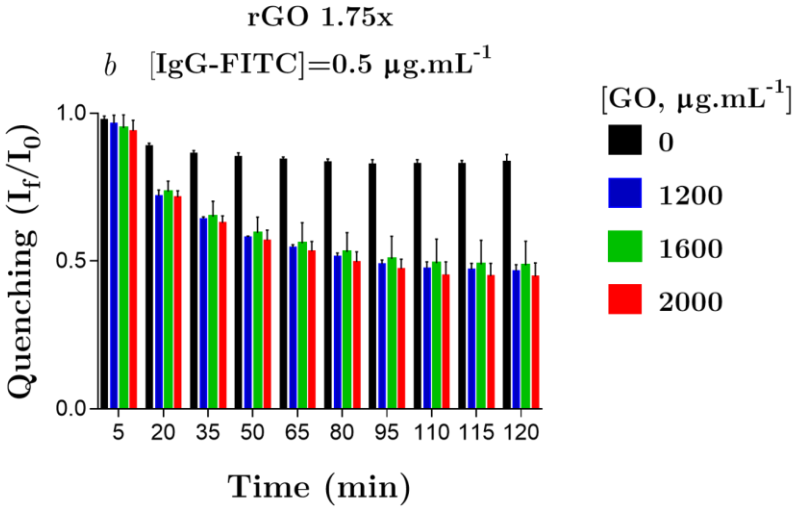

Figure A- 7 Fluorescence quenching bar graphs.

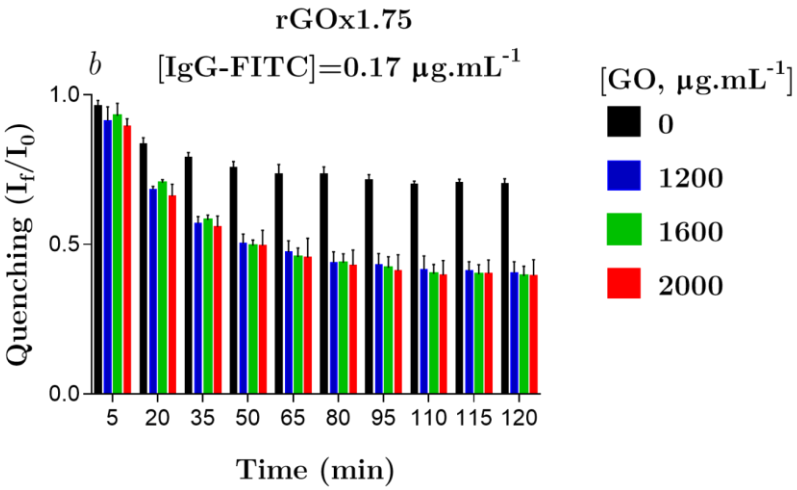

Figure A- 8 Fluorescence quenching bar graphs.

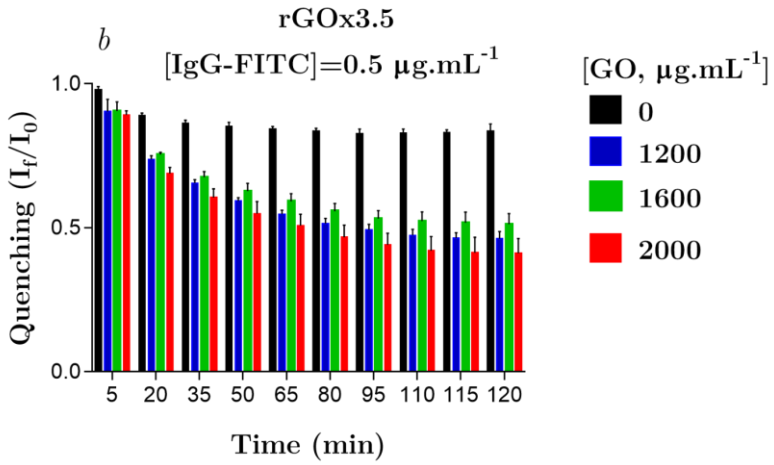

Figure A- 9 . Fluorescence quenching bar graphs.

.

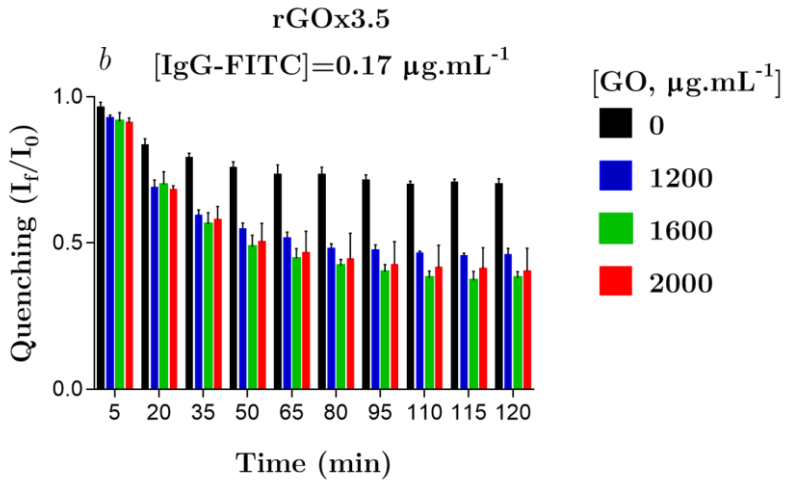

Figure A- 10 Fluorescence quenching bar graphs.

6.5. Laboratorio de Catálisis CFATA-UNAM

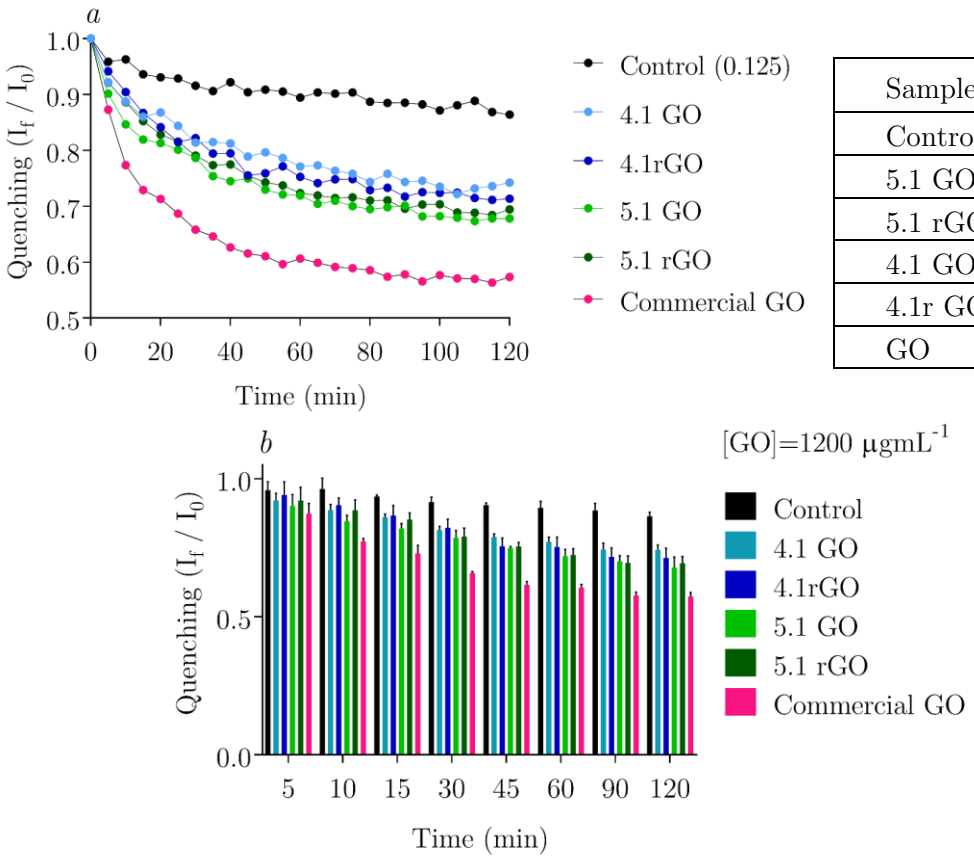

Sample	I_f/I_0
Control	0.86
5.1 GO	0.58
5.1 rGO	0.62
4.1 GO	0.65
4.1r GO	0.55
GO	0.48

Figure A- 11 Kinetics of fluorescence quenching for different samples of GO/rGO on TCT microplate surface. b. Fluorescence quenching bar graphs. ([IgG-FITC]=0.125 µg mL-1)

4.1 GO/rGO sample

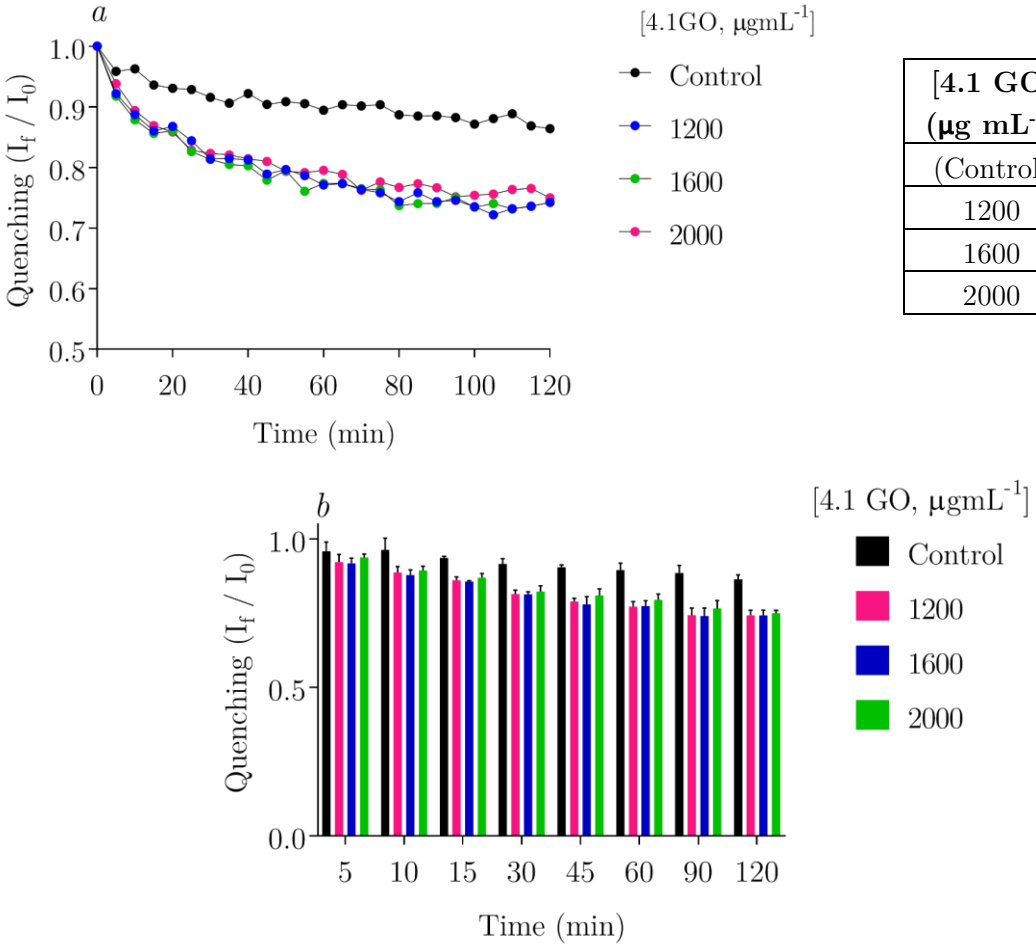

[4.1 GO] (μg mL^{-1})	I_f/I_0
(Control)	0.86
1200	0.74
1600	0.74
2000	0.75

Figure A- 12 Kinetics of fluorescence quenching for different concentrations of 4.1GO on TCT microplate surface. b. Fluorescence quenching bar graphs. ([IgG-FITC]=0.125 μg mL^{-1})

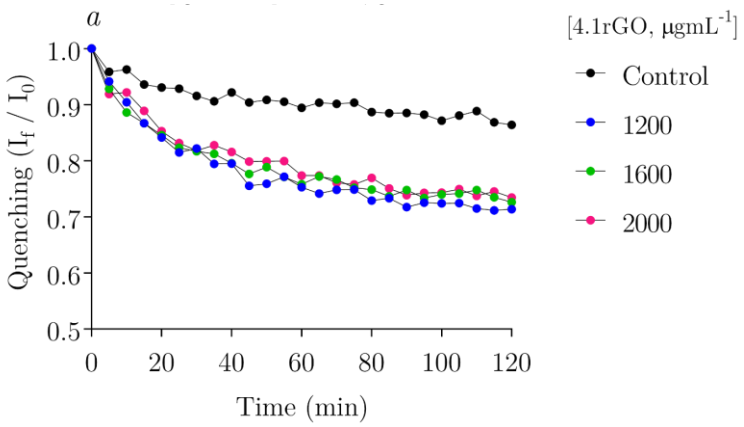

[4.1 rGO] (μg mL^{-1})	I_f/I_0
Control	0.86
1200	0.71
1600	0.73
2000	0.73

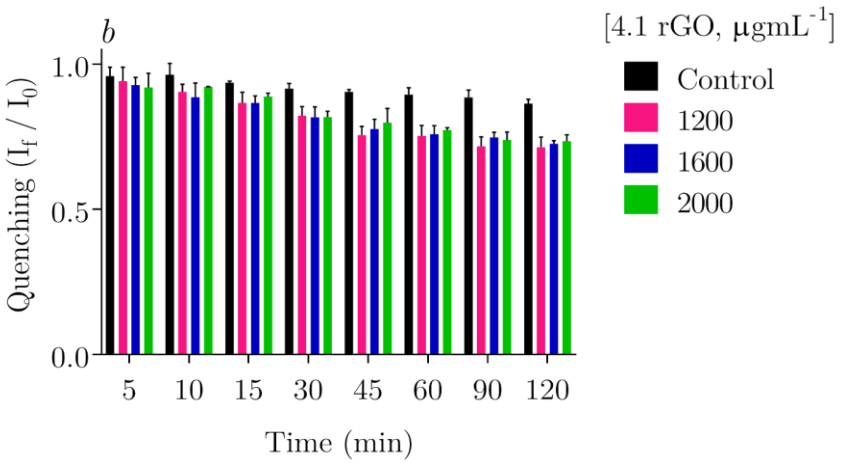

Figure A- 13 Kinetics of fluorescence quenching for different concentrations of 4.1GO on TCT microplate surface. b. Fluorescence quenching bar graphs. ([IgG-FITC] =0.125 μg mL-1)

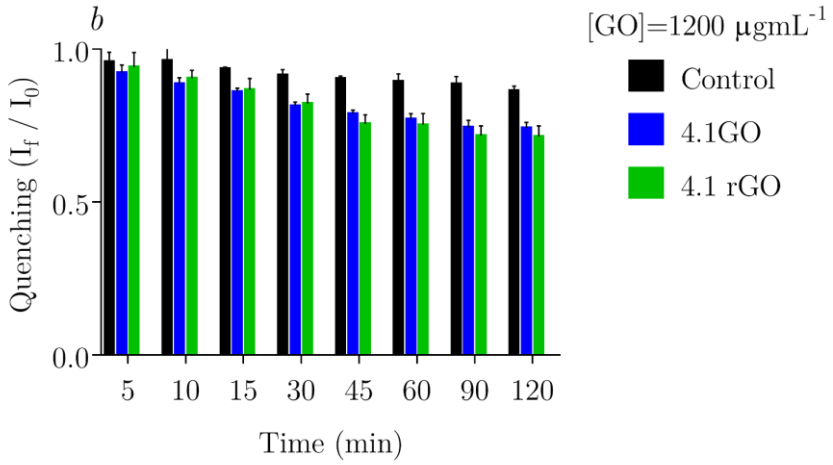

Figure A- 14 Kinetics of fluorescence quenching using samples of 4.1 GO and 4.1 rGO on TCT microplate surface. b. Fluorescence quenching bar graphs. ([GO] = 1200 μg mL-1, [IgG-FITC]=0.125 μg mL-1)

5.1 GO/rGO sample

For this sample, the photoluminescence quenching results showed in Figure A-15 for different concentrations of 5.1 GO and [IgG-FITC] = 0.125 μg. mL^{-1} indicated that 1200 μg mL^{-1} is the concentration most efficient quencher.

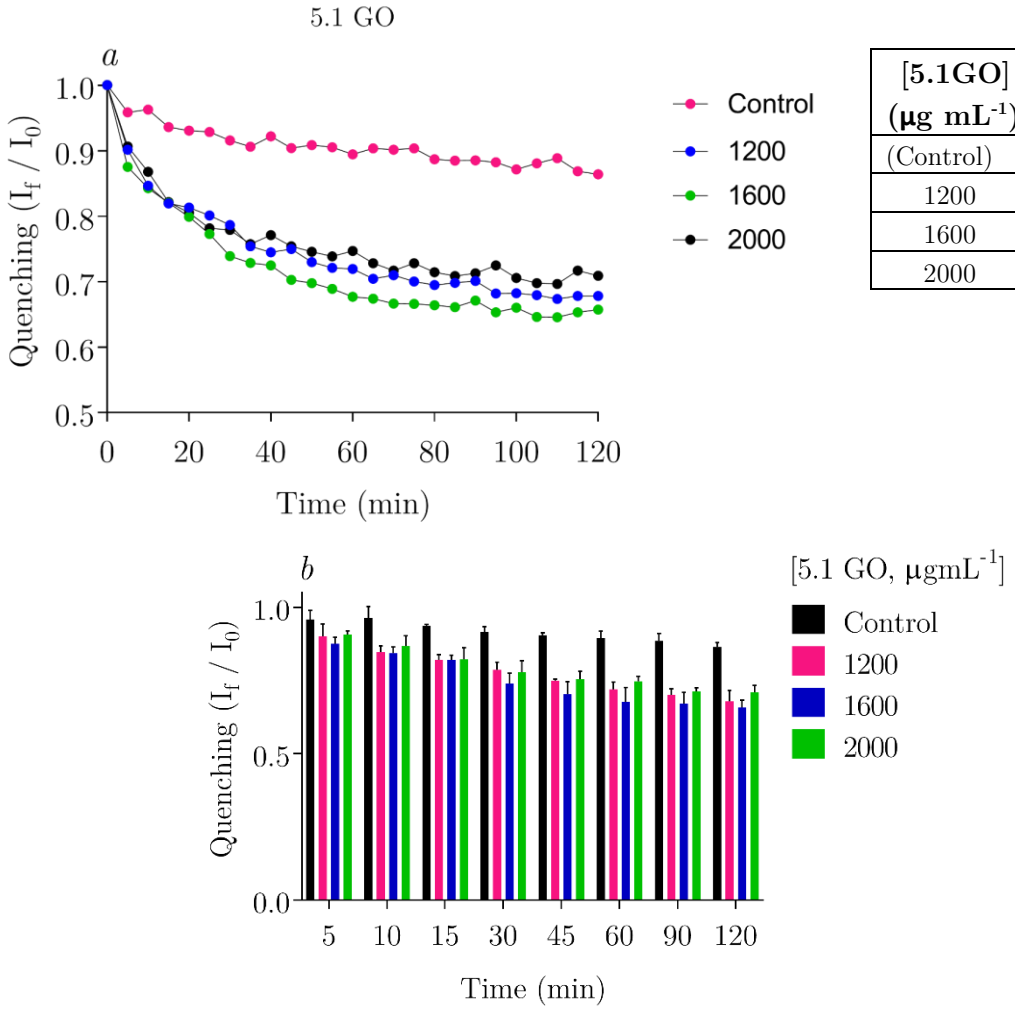

[5.1GO] (μg mL^{-1})	**I_f/I_0**
(Control)	0.86
1200	0.67
1600	0.66
2000	0.71

Figure A- 15 Kinetics of fluorescence quenching using samples of 5.1GO and 5.1rGO on TCT microplate surface. b. Fluorescence quenching bar graphs. ([IgG-FITC] =0.125 μg mL-1)

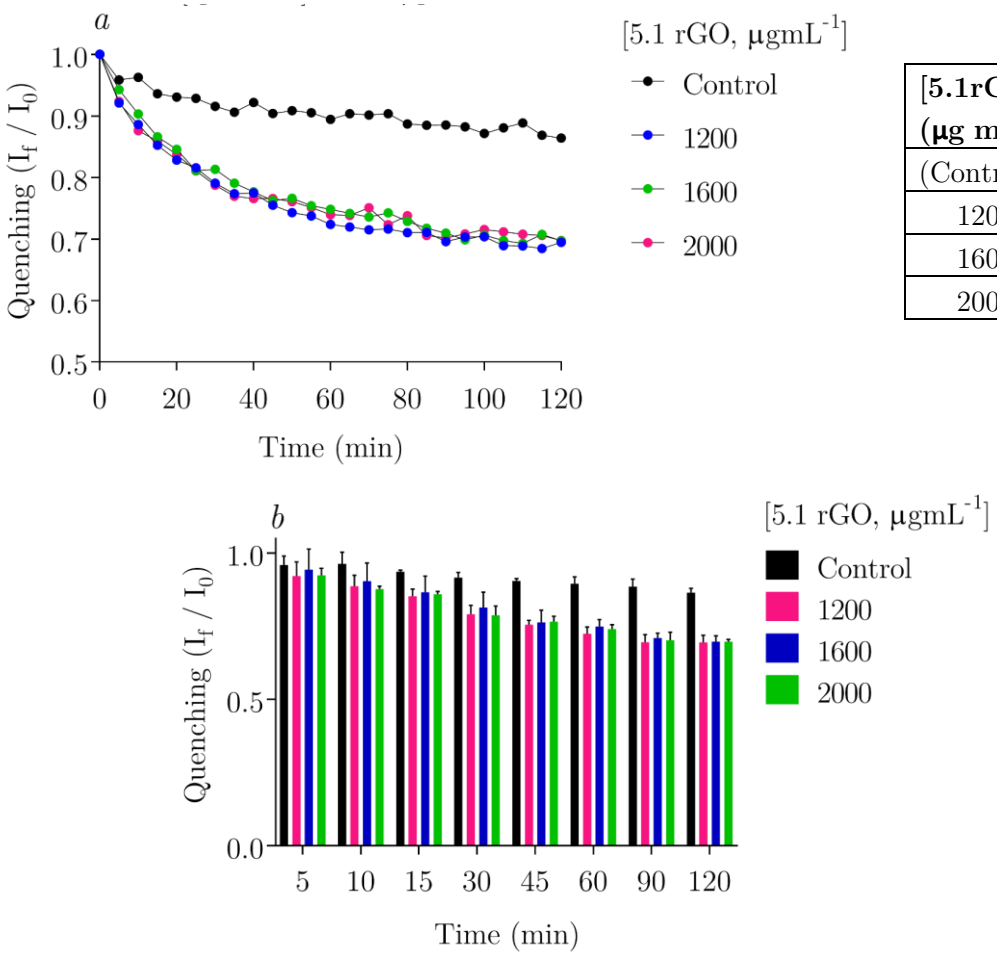

[5.1rGO] (μg mL^{-1})	**I_f/I_0**
(Control)	0.86
1200	0.69
1600	0.70
2000	0.70

Figure A- 16 Kinetics of fluorescence quenching using samples of 5.1GO and 5.1rGO on TCT microplate surface. b. Fluorescence quenching bar graphs. ([IgG-FITC] =0.125 μg mL-1)

According to the results showed above, the GO/rGO samples synthesized by the CFATA research group presented greater efficiency in in the attaching process when these were adhered to the high binding surface than to the TCT surface. This is reflected in the fact that the abilities as fluorescence quencher enhance when the surface employed was that of high binding.

6.5.1. High binding microplate surface

According to Figure A-17a, the study on the surface of high binding microplates, indicates a similarity between the quenching of the coated surfaces with the GO concentrations of 1200 and 1600 μg mL^{-1}. Fluorescence quenching in this surface is no better than on the polystyrene surfaces of the TCT microplates, at least for the GO commercial case.

Additionally, the surface covered with the GO concentration of 2000 μg mL^{-1} presents an inefficient quenching.

The error bars in Figure A-17 b, display the instability of the system when this surface is covered with commercial GO.

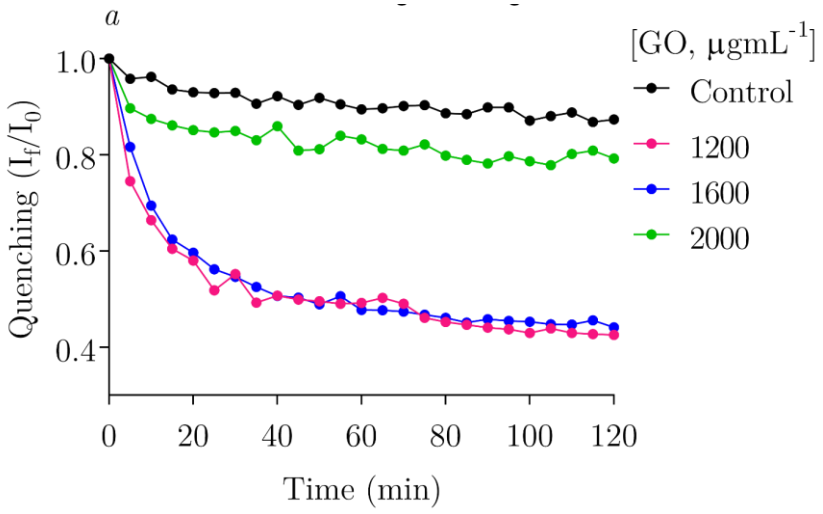

[GO] (μg mL^{-1})	I_f/I_0
(Control)	0.87
1200	0.43
1600	0.44
2000	0.78

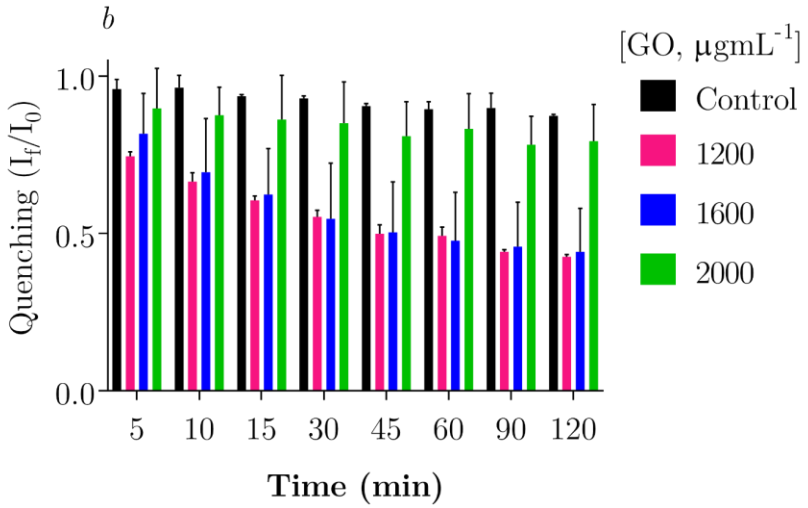

Figure A- 17 a. Kinetics of fluorescence quenching for different samples of GO/rGO on high binding microplate surface. b. Fluorescence quenching bar graphs. ([IgG-FITC] =0.125 μg mL-1)

4.1 GO/rGO and 5.1 GO/rGO samples (bar graphs).

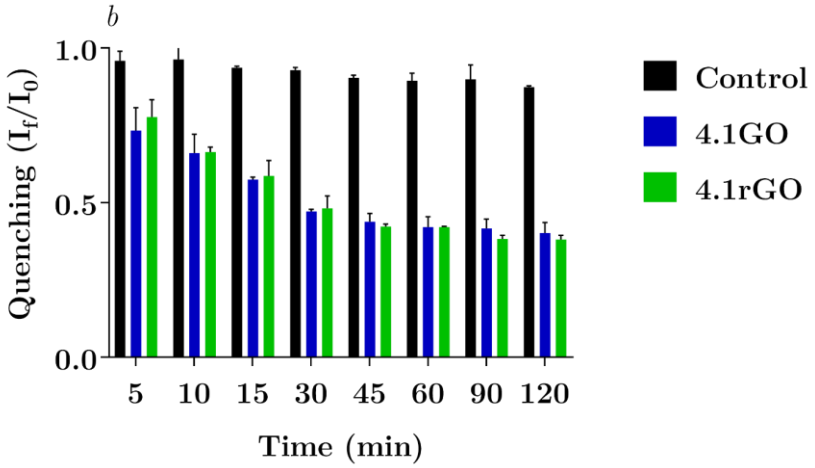

Figure A- 18 Kinetics of fluorescence quenching using samples of 4.1 GO and 4.1rGO on High binding microplate surface. b. Fluorescence quenching bar graphs. ([GO] = 1200 µg mL-1, [IgG-FITC] =0.125 µg mL-1)

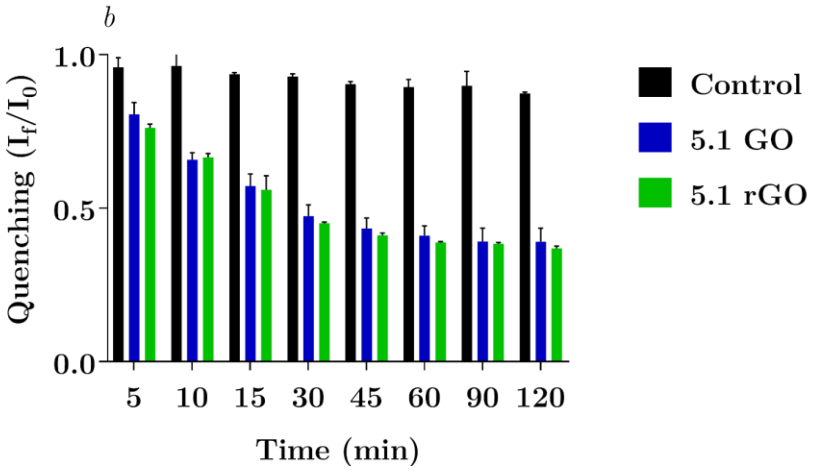

Figure A- 19 Kinetics of fluorescence quenching using samples of 5.1GO and 5.1 rGO on High binding microplate surface. b. Fluorescence quenching bar graphs. ([GO] = 1200 µg mL^{-1}, [IgG-FITC]=0.125 µg mL^{-1})

6.6.Fitting parameter χ^2

TCT microplate surface

4.1[GO] ($\mu g.mL^{-1}$)	1200	1600	2000
χ^2	0.9112	0.9085	0.9334

4.1[rGO] ($\mu g.mL^{-1}$)	1200	1600	2000
χ^2	0.8744	0.8713	0.9172

5.1[GO] ($\mu g.mL^{-1}$)	1200	1600	2000
χ^2	0.924	0.8518	0.8718

5.1[rGO] ($\mu g.mL^{-1}$)	1200	1600	2000
χ^2	0.9272	0.8914	0.9212

High binding microplate surface

4.1[GO] ($\mu g.mL^{-1}$)	1200	1600	2000
χ^2	0.9557	0.9688	0.982

4.1[rGO] ($\mu g.mL^{-1}$)	1200	1600	2000
χ^2	0.9799	0.9872	0.9871

5.1[GO] ($\mu g.mL^{-1}$)	1200	1600	2000
χ^2	0.9603	0.8871	0.9659

5.1[rGO] ($\mu g.mL^{-1}$)	1200	1600	2000
χ^2	0.9897	0.9279	0.9873

rGO (commercially available)

1.75×[GO] - [IgG-FITC, μg. mL^{-1}]

[GO] (μg.mL^{-1})	χ^2	
	0.5	0.17
1200	0.9846	0.9693
1600	0.8748	0.9792
2000	0.95	0.9427

3.5×[GO] - [IgG-FITC, μg. mL^{-1}]

[GO] (μg.mL^{-1})	χ^2	
	0.5	0.17
1200	0.9794	0.9855
1600	0.959	0.9773
2000	0.9474	0.9863